

Dark matter bound-state formation in the Sun

Xiaoyong Chu,^{1,*} Raghuv eer Garani,^{2,†} Camilo García-Cely,^{3,‡} and Thomas Hambye^{4,5,§}

¹*Institute of High Energy Physics, Austrian Academy of Sciences,*

Nikolsdorfer Gasse 18, 1050 Vienna, Austria

²*INFN Sezione di Firenze, Via G. Sansone 1, I-50019 Sesto Fiorentino, Italy*

³*Instituto de Física Corpuscular (IFIC), Universitat de València-CSIC,*

Parc Científic UV, C/ Catedrático José Beltrán 2, E-46980 Paterna, Spain

⁴*Service de Physique Théorique Université Libre de Bruxelles,*

Boulevard du Triomphe, CP225, 1050 Brussels, Belgium

⁵*CERN, Theoretical Physics Department, Geneva, Switzerland*

The Sun may capture asymmetric dark matter (DM), which can subsequently form bound-states through the radiative emission of a sub-GeV scalar. This process enables generation of scalars without requiring DM annihilation. In addition to DM capture on nucleons, the DM-scalar coupling responsible for bound-state formation also induces capture from self-scatterings of ambient DM particles with DM particles already captured, as well as with DM bound-states formed in-situ within the Sun. This scenario is studied in detail by solving Boltzmann equations numerically and analytically. In particular, we take into consideration that the DM self-capture rates require a treatment beyond the conventional Born approximation. We show that, thanks to DM scatterings on bound-states, the number of DM particles captured increases exponentially, leading to enhanced emission of relativistic scalars through bound-state formation, whose final decay products could be observable. We explore phenomenological signatures with the example that the scalar mediator decays to neutrinos. We find that the neutrino flux emitted can be comparable to atmospheric neutrino fluxes within the range of energies below one hundred MeV. Future facilities like Hyper-K, and direct DM detection experiments can further test such scenario.

* xiaoyong.chu@oeaw.ac.at

† garani@fi.infn.it

‡ camilo.garcia@ific.uv.es

§ thomas.hambye@ulb.be

CONTENTS

I. Introduction	2
II. Number evolution of DM particles	3
A. Determination of the various rates	5
B. Integrating the Boltzmann equations	10
III. Neutrino flux and Terrestrial detection	13
IV. Results and constraints for an explicit model	14
A. Model	14
B. Constraints and results	15
V. Summary	19
A. Approximate parametric solution to number evolution of DM particles	20
1. Case with no self-capture on DM bound-states	21
2. Case with self-capture on DM bound-states	22
B. (Non-)perturbative treatment of elastic DM scattering	24
1. Integrated DM self-scattering in DM halos	25
2. Differential DM-DM(BS) scattering for DM capture	26
C. DM thermalization	28
References	29

I. INTRODUCTION

Wherever dark matter (DM) particles are numerous, it is possible that two or more of them form bound-states [1–20]. This could occur if DM undergoes attractive self-interactions mediated by a scalar or vector boson. In this case bound-state formation (BSF) can occur radiatively via the emission of this mediator, leading to an observable flux of particles. Indirect signals of BSF in the center of the Milky Way has been studied for DM with no particle-antiparticle asymmetry, as well as for asymmetric DM [20–23]. In this work we consider the possibility that the BSF process occurs in the Sun and study the corresponding DM indirect detection signals.

Symmetric DM accumulating in the Sun from its capture on nucleons and their corresponding indirect detection signals due to emitted meta-stable mediators have been studied in numerous works, see e.g. [24–41]. In these scenarios, the accumulation of DM particles in the Sun reaches a saturation point when the annihilation rate matches the capture rate. This is not the case of asymmetric DM scenarios as DM cannot annihilate. Interestingly, this absence of annihilation permits a greater accumulation of DM particles. However, it comes with the drawback of not generating any indirect detection signal.

The BSF of asymmetric DM particles in the Sun from radiative emission of a light scalar has the interesting property of allowing both DM indirect detection and large accumulation of DM particles in the Sun. A crucial aspect of this scenario is that the DM-scalar interaction that is needed for BSF inherently implies that DM capture results not only from interactions with nucleons but also from interactions with previously accumulated DM particles and DM bound-states (DMBS). This means that the capture rate is larger than that of the usual symmetric or asymmetric scenarios in which the capture only arises from DM-nucleon scatterings. This allows for a larger accumulation and an enhanced flux of emitted particles. To quantify this effect, it will be necessary to compute the rates for DM-DM and DM-DMBS scatterings, which –as we will show– receive non-perturbative contributions which can be calculated in the semi-classical approximation. To our knowledge this possibility that asymmetric DM particles form bound-states in the Sun and that DM particles are captured by scattering off DM bound-states has not been considered before.¹

For concreteness, in this work we assume that the associated light scalars, once emitted when the bound-states form, decay into SM particles, in particular to neutrinos. As is well known, unlike other SM particles, low energy neutrinos can escape the Sun leading to observable signatures even if the decay takes place inside the Sun. After solving the set of Boltzmann equations that describe the dynamics of DM accumulation in the Sun in section II, we show in section III that an observable neutrino flux could arise from the decays of the emitted mediator via the BSF of those accumulated DM. Finally, in section IV we discuss relevant constraints from both astrophysical observations and terrestrial experiments, such as DM self-interactions, BBN, CMB, and direct/indirect searches.

II. NUMBER EVOLUTION OF DM PARTICLES

Before considering quantitatively any concrete model, this section introduces the basic relevant processes and related Boltzmann equations determining the number of DM particles captured in

¹ Particle-antiparticle BSF inside the Sun for symmetric DM was considered in [14].

the Sun. The framework of our interest is based on an interaction between the DM particle and a lighter particle. For definiteness in the following we consider that DM is made of Dirac fermions χ , with a Yukawa coupling g_s to a lighter scalar particle ϕ

$$\mathcal{L} \supset -g_s \phi \bar{\chi} \chi. \quad (1)$$

To assume a scalar mediator is convenient because it induces an attractive interaction.² We also assume that DM is asymmetric, thus it does not annihilate in the present epoch. Nevertheless, in addition to the usual capture due to scattering on target nuclei (C_\star) [44, 45], three additional terms come into play in the Boltzmann equation determining the DM particle number N_χ , due to DM- ϕ interactions. First, depending on the strength of self-interaction, DM particles could efficiently form χ - χ bound-states by emitting the particle mediating DM self-interactions. The rate of the latter is denoted by A_{bsf} . Since the number of free particles is reduced by two per process, the term $-2 \cdot \frac{1}{2} A_{\text{bsf}} N_\chi^2$ is introduced in the equation that describes the evolution of N_χ , where the second factor, $\frac{1}{2}$, counts for double-counting of identical initial states. In contrast to the case of annihilation, in this scenario DM particles are not lost by the system. In effect, there is a build-up of DM bound-states within the celestial body, whose number $N_{2\chi}$ is determined by a second Boltzmann equation that simply involves a $+\frac{1}{2} A_{\text{bsf}} N_\chi^2$ term. Second, there is a term coming from capture of Galactic DM on already-captured DM particles, whose rate is denoted by C_χ . Finally, there is a term from capture of Galactic DM on the formed bound-states, denoted by $C_{2\chi}$. The presence of both C_χ and $C_{2\chi}$ terms increase DM accretion. In summary, both populations evolve according to the following set of differential equations,

$$\frac{dN_\chi}{dt} = C_\star - A_{\text{bsf}} N_\chi^2 + C_\chi N_\chi + C_{2\chi} N_{2\chi}, \quad (2)$$

$$\frac{dN_{2\chi}}{dt} = \frac{1}{2} A_{\text{bsf}} N_\chi^2. \quad (3)$$

The various rates C_\star , C_χ and $C_{2\chi}$ take into account the fact that the three kinds of DM capture occur within different spheres around the solar center. Here we have neglected self-capture via direct BSF between a galactic DM and a captured DM particle, as such inelastic scattering is typically much weaker than the elastic scattering with two DM initial states. Also, in these Boltzmann equations we do not write down explicitly additional terms coming from possible evaporation of the captured DM particles. We have checked that the DM mass above which evaporation is negligible is not significantly different than in the standard scenario (no-self interaction effects).

² Such interactions do not result in the formation of mini black hole in the Sun, i.e. the Chandrasekhar limit for fermions is not modified [42, 43].

The value is found to be $m_{\text{evap}} \approx 5$ GeV, which is about 50% larger than that in the standard scenario [34]. Therefore, in the following phenomenological discussion we consider only DM masses above 5 GeV. Once DM particles are captured they thermalize with the solar material, leading to efficient formation of bound-states. We always assume that the thermalization happens quickly, and refer to Appendix C for detailed calculation of the thermalization process.

The number of DM particles captured in any of the three ways cannot be larger than the corresponding geometric rates, as the latter assume that all DM particles crossing the corresponding thermal spheres are captured. This is taken into account through the following conservative matching for the regimes of small optical depth (thin) to large (thick)³

$$C_\chi N_\chi \rightarrow C_\chi N_\chi \Theta(C_\chi^g - C_\chi N_\chi) + C_\chi^g \Theta(C_\chi N_\chi - C_\chi^g), \quad (4)$$

$$C_{2\chi} N_{2\chi} \rightarrow C_{2\chi} N_{2\chi} \Theta(C_{2\chi}^g - C_{2\chi} N_{2\chi}) + C_{2\chi}^g \Theta(C_{2\chi} N_{2\chi} - C_{2\chi}^g). \quad (5)$$

where the respective geometric rates on the DM and DMBS thermal spheres are denoted by C_χ^g and $C_{2\chi}^g$. These geometric rates determine the maximal possible capture rates, independently of the underlying particle model.

Note that we do not consider bound-states containing more than two χ particles, under the assumption that there exist bottlenecks to form heavier bound-states, such as fast decays of $(3\chi) \rightarrow (2\chi) + \chi$ and $(4\chi) \rightarrow (2\chi) + (2\chi)$. See e.g. [46–49] for further discussions. In practice, if there is formation of many-body bound-states, each captured DM particle may cause the emission of a few more mediator particles while thermal radii for heavier bound-states shrink by a factor of few. The total effect at most modifies our results mildly.⁴

We begin in the next subsection by determining the various rates. The reader seeking immediate understanding of their interplay in the Boltzmann equations can directly refer to section II B.

A. Determination of the various rates

a. Thermal radius and geometric rates C_\star^g , C_χ^g and $C_{2\chi}^g$: Once a DM particle has been captured in the Sun, or a DMBS has formed, these particles will thermalize with the SM material of the Sun and lie within different spheres of thermal radius r_{th} . Noting that the mass of a bound-state is approximately twice that of a DM particle, these radii are obtained [44, 50] by equating the average

³ These equations are accurate if only one geometric rate can be saturated. This will be the case studied here, for which the geometric capture rates on free DM (C_χ^g) and on nucleons (C_\star^g) are never reached.

⁴ The presence of stable many-body bound-states, as well as self-capture via inelastic scattering, may reduce DM evaporation efficiency by quickly capturing free χ particles into heavier bound-states. This can have qualitative consequences for DM candidates below GeV or those captured by Earth, which is left for a future study.

thermal energy, $3T_\odot/2$, to the gravitational potential energy per particle, $2\pi Gr_{\text{th}}^2\rho_\odot nm_\chi/3$, as

$$r_{\text{th}} = \left(\frac{9T_\odot}{4\pi G\rho_\odot nm_\chi} \right)^{\frac{1}{2}} = 0.03R_\odot \left(\frac{T_\odot}{2.2 \text{ keV}} \frac{150 \frac{\text{g}}{\text{cm}^3}}{\rho_\odot} \frac{10 \text{ GeV}}{nm_\chi} \right)^{\frac{1}{2}}, \quad \text{with } n = 1(2) \text{ for DM (DMBS)}. \quad (6)$$

That is, the DM bound-state thermal radius is smaller than the DM thermal radius by a factor of $\sqrt{2}$. We take the solar core temperature, T_\odot , to be 2.2 keV, and the core mass density to be $\rho_\odot \sim 150 \text{ g/cm}^3$. For example, the thermal radius of 3 GeV DM particles is about one-tenth of the Solar radius, $R_\odot \simeq 6.9 \times 10^5 \text{ km}$ [51]. In addition, we will assume throughout that the DM radial distribution is isothermal, with its temperature $T \approx T_\odot$ [44, 52].

Upon taking into account the relative motion of the Sun with respect to the galactic DM halo, the geometric capture rate on nucleons is [53]

$$C_\star^g = \frac{\rho_\chi}{m_\chi} \pi R_\odot^2 \bar{v} \simeq 6 \times 10^{28} \text{ s}^{-1} \left(\frac{\rho_\chi}{0.3 \text{ GeV/cm}^3} \cdot \frac{10 \text{ GeV}}{m_\chi} \right). \quad (7)$$

Here \bar{v} is a factor with units of velocity, accounting for the relative motion of the Sun and the velocity distribution of DM, see e.g. [52]. Throughout this work we take the local DM density $\rho_\chi = 0.3 \text{ GeV/cm}^3$. Apparently, the geometric capture rate is proportional to the corresponding cross-sectional area. So this expression can be rescaled to obtain the geometric rate for DM self-capture on DM and on DMBS (i.e. when the mean free path of DM is smaller than the corresponding thermal sphere) by adding the corresponding factor $(r_{\text{th}}/R_\odot)^2$. This results in geometric self-capture rates which scale as m_χ^{-2} ,

$$C_\chi^g = 5 \times 10^{25} \text{ s}^{-1} \left(\frac{10 \text{ GeV}}{m_\chi} \right)^2, \quad C_{2\chi}^g \approx 2.6 \times 10^{25} \text{ s}^{-1} \left(\frac{10 \text{ GeV}}{m_\chi} \right)^2. \quad (8)$$

b. Capture on nucleons rate C_\star : The capture rate of DM particles in the Sun has been well studied in the literature. It can be written as [25]

$$C_\star \approx \sum_i \int_0^{R_\odot} 4\pi r^2 n_i(r) dr \int_0^\infty du_\chi \left(\frac{\rho_\chi}{m_\chi} \right) \times u_\chi \omega^2(r) f_\odot(u_\chi) \int_{E_R^{\text{min}}}^{E_R^{\text{max}}} \frac{d\sigma_i}{dE_R} dE_R, \quad (9)$$

where $f_\odot(u_\chi)$ is the normalized asymptotic DM velocity distribution far from the Sun in the solar frame. The values of radial number density distribution of each element i , denoted as $n_i(r)$ above, are adopted from the AGSS09 Solar model [51]. Together with the escape velocity at a distance r away from the centre of the Sun, $v_e(r)$, it provides the relative velocity of a DM particle when it scatters with the nucleus, $\omega(r) = \sqrt{u_\chi^2 + v_e(r)^2}$. The differential cross section, $d\sigma_i/dE_R$, encodes the energy dependence of elastic scattering between DM and nucleus i in the non-relativistic limit. The recoil energy in the solar frame is given by $E_R = \mu_{\chi N}^2/m_N \times \omega^2(1 - \cos \theta_{CM})$,

where $\mu_{\chi N} = m_\chi m_N / (m_\chi + m_N)$ is the reduced mass of the DM-nucleus system. For the Solar capture to actually occur, we need to make sure that the recoil energy lies within the range of $E_R^{min} < E_R < E_R^{max}$, with

$$E_R^{min} = \frac{1}{2} m_\chi u_\chi^2, \quad E_R^{max} = \frac{2\mu_{\chi N}^2 \omega^2}{m_N}. \quad (10)$$

For definiteness we assume that the dark sector communicates with the SM particles through the Higgs portal, and that the light mediator ϕ mixes with the Higgs boson with a mixing angle θ_ϕ .

The differential cross section in the Born approximation is then

$$\frac{d\sigma}{dE_R} = \frac{g_s^2 \cos^2 \theta_\phi \sin^2 \theta_\phi}{2\pi} \frac{m_N^2 f_N^2}{v_H^2} \frac{m_N}{\omega^2 (2m_N E_R + m_\phi^2)^2} F^2 \left(\frac{E_R}{Q_0} \right), \quad (11)$$

where $F(E_R/Q_0)$ is the Helm form factor and $f_N = f_u^N + f_d^N + f_s^N + 6/27 f_G$, which is an $\mathcal{O}(1)$ number (see e.g. [54, 55]).

The DM capture rates on nucleons are shown in Fig. 1, corresponding to a Higgs mixing angle $\sin \theta_\phi = 10^{-10}$ and $g_s = 1$, for several mediator masses (labeled in red). The geometric capture and self-capture rates, Eq. (7) and (8), are shown as black dashed and dotted curves. For mediator mass below MeV the differential cross section is independent of the mediator mass since $m_N E_R^{max} \sim \mu_{\chi N} v_e^2$, which is above MeV for $m_\chi \geq m_{\text{evap}}$. This leads to a t -channel enhancement, which in the $m_\chi \gg m_N$ limit gives a capture cross section scaling as m_χ^{-1} , leading to a capture rate scaling as m_χ^{-2} . While, for mediator masses larger than ~ 100 MeV and $m_\chi \lesssim m_N$, the capture rate in turn scales as m_χ . Note that in Eq. (11) we have neglected the effect of DM-electron scattering, which is subleading due to lower energy loss and tiny electron Yukawa coupling.

c. Bound-state formation rate A_{bsf} As stated above, we consider DM to be asymmetric and made of Dirac fermions (χ). The interaction between two (identical) DM particles is attractive when the mediator is a scalar (ϕ), with a classical Yukawa potential $V(r) = -\frac{\alpha}{r} e^{-m_\phi r}$. The binding energy of the bound-state is $E_{\text{bind}} \simeq \frac{m_\chi \alpha^2}{4} - \alpha m_\phi$, with the dark coupling $\alpha \equiv g_s^2 / 4\pi$. From the merging of two identical fermions, the radiative BSF rate has been estimated in [56], yielding

$$\sigma_{\text{BSF}v} \simeq \frac{256\pi^2 \alpha^5}{5e^4 m_\chi^2 v_{\text{rel}}}, \quad (12)$$

in the limit of $\alpha/v_{\text{rel}} \gg 1$ and $m_\phi \rightarrow 0$, where the DM relative velocity is $v_{\text{rel}} \simeq 2v_{\chi, \odot}$. The recoil velocity of the DMBS is $\alpha^2/8$ in this limit, which must be below the escape velocity from the Solar center, resulting in the requirement $\alpha \lesssim 0.18$.⁵ Finally, the total annihilation rate that enters the

⁵ Due to velocity enhancement, the BSF process in the early Universe could be efficient such that very few free DM particles could exist in the current epoch. Then qualitative changes in some regions of parameter space of interest are expected. However, this depends on the assumed cosmological history, and it is not explored in this work. See e.g. [49, 56] for related discussions.

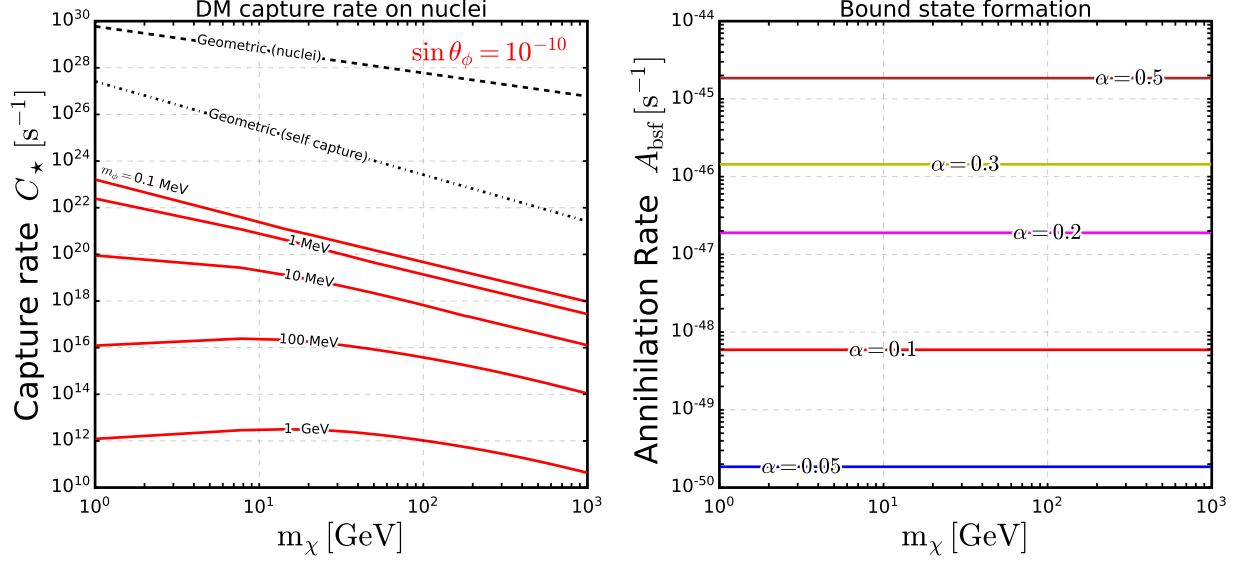


FIG. 1. *Left*: DM capture rate on nucleons for several mediator masses for a Higgs mixing angle $\sin \theta_\phi = 10^{-10}$. The geometric capture on nucleons C_\star^g and C_χ^g self-capture rates are shown by the dashed and dashed-dotted black curves. The $C_{2\chi}^g$ self-capture rate line (not shown) is a factor 2 below the C_χ^g line. *Right*: The DM BSF rate inside the Sun, for several values of α .

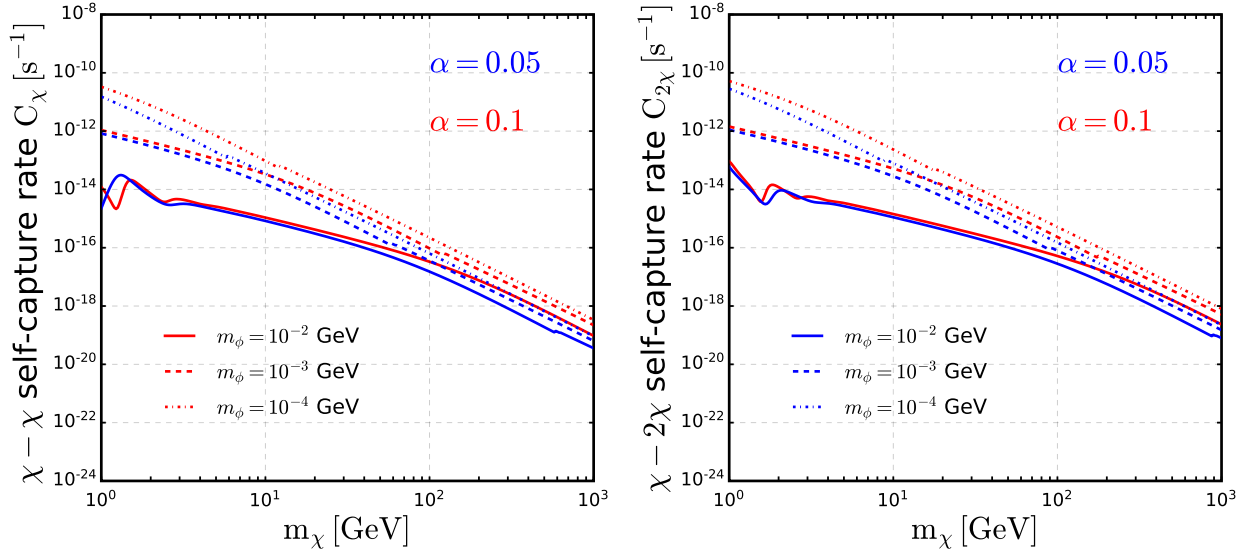


FIG. 2. *Left (right)*: DM self-capture rates due to DM-DM (DM-DMBS) scattering. See text for details.

number evolution equation is given by

$$A_{\text{bsf}} = \frac{\int n_\chi^2 \sigma_{\text{BSF}} v dV}{(\int n_\chi dV)^2}. \quad (13)$$

The normalized DM radial distribution is

$$n_\chi(r, t) = N_\chi(t) \frac{e^{-m_\chi \phi(r)/T}}{\int_0^{R_\odot} e^{-m_\chi \phi(r)/T} 4\pi r^2 dr}, \quad (14)$$

which corresponds to an isothermal sphere, with a radial dependence set by the gravitational potential $\phi(r) = \int_0^r GM_\odot(r')/r'^2 dr'$, with G the gravitational constant and $M_\odot(r')$ the mass inside a sphere of radius r' , and $N_\chi(t)$ is the total population of DM particles at a given time t .

Once DM particles are thermalized its average velocity is $v_\chi \simeq \sqrt{2T/m_\chi}$. The smallness of this value considerably boosts the BSF in Eq. (12): $v_{rel} \simeq 4.2 \times 10^{-3} \sqrt{1 \text{ GeV}/m_\chi}$. Consequently, A_{bsf} scales as $\alpha^5 (m_\chi^2 v_{rel})^{-1} (r_{th}^\chi)^{-3}$, be approximately independent of the DM mass in practice, as shown in right panel of Fig. 1.

d. DM self capture rates C_χ and $C_{2\chi}$: Analogous to DM-nucleon capture rate, we estimate the self-capture rate per target DM particle in the Sun as follows

$$C_\chi = \int_0^{r_{th}^\chi} dr 4\pi r^2 n_\chi(r) \int_0^\infty du_\chi \left(\frac{\rho_\chi}{m_\chi} \right) u_\chi f_\odot(u_\chi) w^2 \int_{\cos\theta_{min}}^{\cos\theta_{max}} \frac{d\sigma_{\chi-\chi}}{d\cos\theta} d\cos\theta. \quad (15)$$

The minimum scattering angle is set by the requirement of a minimum energy that has to be lost in a single scattering event to be captured, i.e. DM kinetic energy at infinity must be smaller than $1/2 m_\chi u_\chi^2$. The maximum scattering angle for scattering of identical particles is $\pi/2$. Therefore $\cos\theta_{min} = 1 - 2\frac{u_\chi^2}{\omega^2}$ and $\cos\theta_{max} = 0$. Similar to the DM-DM self-capture, the capture rate due to DM-DMBS scattering, per target DMBS in the Sun, is given by

$$C_{2\chi} = \int_0^{r_{th}^{2\chi}} dr 4\pi r^2 n_{2\chi}(r) \int_0^\infty du_\chi \left(\frac{\rho_\chi}{m_\chi} \right) u_\chi f_\odot(u_\chi) \omega^2 \int_{\cos\theta_{min}}^{\cos\theta_{max}} \frac{d\sigma_{2\chi-\chi}}{d\cos\theta} F_\chi^2 \left(\frac{E_r}{Q_\chi} \right) d\cos\theta, \quad (16)$$

with $\cos\theta_{min} = 1 - \frac{9}{8} \frac{u_\chi^2}{\omega^2}$ and $\cos\theta_{max} = -1$. We have used $m_{2\chi} \approx 2m_\chi$ and set that the coupling to bound-state is 2α (as the vertex is of the scalar type). We assume that the form factor has the form of $\exp(E_r/Q_\chi)$. The typical size of the bound-state is set by the Bohr radius, hence $Q_\chi = m_\chi \alpha$. To a good approximation $F_\chi \rightarrow 1$ for a typical value of $\alpha = 0.1$. The radial number density of DMBS ($n_{2\chi}$) is assumed to be isothermal, analogous to n_χ .

Bound-state formation suggests that non-perturbative effects are non-negligible for the calculation of the DM self-scattering cross section (see e.g. [57, 58]). This is indeed our case. For the parameter values of interest $\alpha \in [0.02, 0.2]$, $m_\chi > 5 \text{ GeV}$, $\text{MeV} \lesssim m_\phi \ll m_\chi$, and $v \sim v_{esc} \sim 4 \times 10^{-3}$, we are never in the Born regime of self-scattering, for which $m_\chi < m_\phi/\alpha$ or $\alpha \lesssim v$ [59]. As a result, a perturbative expansion of the scattering cross section is not justified here, see left panel of Fig. 7 in Appendix B 1. However, for these parameters above, it is not necessary to solve the Schrödinger equation associated with the non-relativistic DM collisions because the scattering process is typically semi-classical, for which the range of the potential is larger than the DM de Broglie

wavelength, that is, $m_\chi v/m_\phi \gtrsim 1$. In this case classical mechanics can be employed to estimate the scattering cross section.⁶

More importantly, unlike phenomenological studies of DM self-scattering in galaxies and galaxy clusters, where the transfer and viscosity cross sections are relevant, here the differential cross section is needed to calculate the integrated self-capture rates introduced above. This is because DM capture needs that enough initial kinetic energy is lost in a single scattering. This condition is imposed by integrating the differential cross section from minimum possible scattering angle (θ_{\min} , set by required energy loss) to the maximum one where the scattered particle still does not gain enough energy to escape. These limits are explicitly indicated in Eqs. (15) and (16). To calculate the differential cross sections, we follow Refs. [60, 61] and solve the elastic scattering with a Yukawa potential classically. Further discussions and full expressions are presented in Appendix B.

We present the results for DM self capture rates through scattering on free DM particles (DM bound-states) in the left (right) panel of Fig. 2. The rates scale proportionally as m_χ^{-2} for $m_\chi \gg m_\phi$. For moderate values of DM masses the scaling is less steep. Note that the capture rate on bound-states $C_{2\chi}$ is approximately larger by a factor of two with respect to C_χ , due to larger Yukawa coupling induced by bound-states and larger maximal allowed scattering angle that keep both particles gravitationally captured.

B. Integrating the Boltzmann equations

The set of coupled Boltzmann equations of Eqs. (2) and (3) has no closed form analytical solution. In Appendix A we describe at length how they can be solved approximately. We summarize in this subsection the main outcome of this discussion. To this end, in Fig. 3 we present the evolution of both populations for two parameter sets. The evolution of N_χ ($N_{2\chi}$) from the numerical integration of the full Boltzmann Eqs. (2) and (3) are given by the solid (dashed) red curves. Curves with other colors correspond to what is obtained switching off both the C_χ and $C_{2\chi}$ terms (black), or only the C_χ term (blue) or only the $C_{2\chi}$ term (green).

At early times the number of free particles N_χ grows as $C_\star t$ (i.e. red and black solid lines coincide). As N_χ increases, the BSF starts to occur efficiently and the corresponding term (quadratic in N_χ) quickly catches up with the constant term associated with capture on nucleons, so that in absence of the $C_{2\chi}$ term, a quasi-static equilibrium between both terms is reached (see black and green solid curves in Fig. 3). Solving the Boltzmann equation for N_χ one gets that the associated

⁶ A precise treatment would require to solve the phase shift for a large number of partial waves, see e.g. [24, 57, 58].

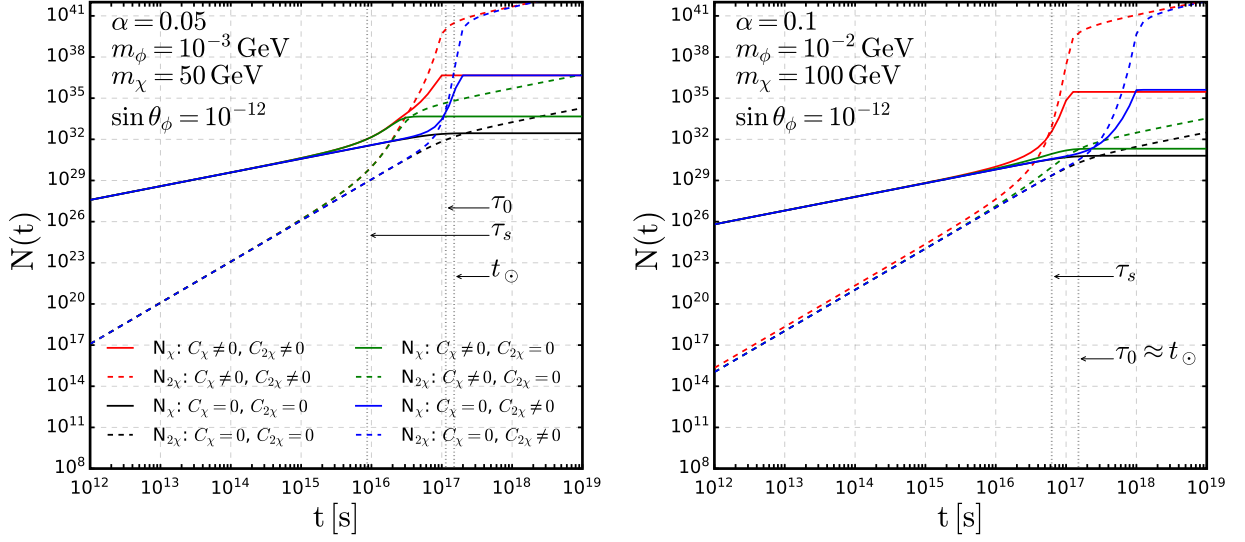


FIG. 3. Number evolution of DM and DM bound-states for two parameter sets, as a function of time. Here τ_s and τ_0 are characteristic times explained in the main text (and exactly defined in Appendix A), t_\odot is the age of the Sun. The color code of the curves in the left panel are the same as that in the right panel.

time scale is $\tau_0 \equiv (C_\star A_{\text{bsf}})^{-1/2}$ if one drops the C_χ term –which has a subleading effect (black solid curve)– or $\tau_s \equiv (C_\star A_{\text{bsf}} + C_\chi^2/4)^{-1/2}$ if one includes it (green solid curve). For more details, see the end of this section and Appendix A.

Another consequence of efficient BSF is that the number of bound-states $N_{2\chi}$ quickly catches up to the number of DM particles N_χ , and never stops growing thereafter, as it is not counterbalanced by any other term in Eq. (3). From this point, the term associated with the capture on bound-states, $C_{2\chi}N_{2\chi}$, takes over and leads to an exponential growth of N_χ (red and blue solid curves in Fig. 3) and of $N_{2\chi}$ (dashed curves with same colors). The exponential growth become significant at $t \gtrsim \tau_s + C_{2\chi}^{-1}$, or at $\tau_0 + C_{2\chi}^{-1}$, depending on whether one includes the C_χ term. This growth lasts until the capture rate saturates the geometric rate within the bound-state thermal sphere, i.e. when the term $C_{2\chi}N_{2\chi}$ reaches $C_{2\chi}^g$. This happens when the mean free path of DM particles becomes much smaller than the bound-state thermal radius. At this moment, we can safely neglect the $C_\chi N_\chi$ term as $N_\chi \ll N_{2\chi}$, thus the Boltzmann equation takes the form, $dN_\chi/dt \simeq C_\star + C_{2\chi}^g - A_{\text{bsf}}N_\chi^2$. This means that, quickly after the geometric capture rate is saturated, the BSF term compensates the constant capture rate from both nucleon and bound-state terms. Setting $dN_\chi/dt \simeq 0$ gives the maximum final value

$$N_{\chi,\text{eq}} \simeq \left(\frac{C_\star + C_{2\chi}^g}{A_{\text{bsf}}} \right)^{1/2}. \quad (17)$$

We denote as τ_g the time when N_χ freezes in such a way. An analytic approximation is given in Appendix A.

Note that, contrary to the $C_{2\chi}N_{2\chi}$ term –which saturates the geometric rate $C_{2\chi}^g$ – the average DM density within the thermal radius r_{th}^χ is smaller than the DMBS density within $r_{\text{th}}^{2\chi}$, so the self-capture term $C_\chi N_\chi$ does not reach C_χ^g at $t = \tau_g$, and will never reach it after, as N_χ stops increasing. As for $N_{2\chi}$, it keeps increasing in time forever. For $t > \tau_g$, it increases linearly in time and the rate of BSF is half the capture rate,

$$\Gamma(t) = \frac{dN_{2\chi}}{dt} = \frac{1}{2}A_{\text{bsf}}N_{\chi,\text{eq}}^2 \simeq \frac{C_\star + C_{2\chi}^g}{2}, \quad (18)$$

inducing a flux of mediators given by the same rate.

The reason why the C_χ term has a subleading effect with respect to the effect of the $C_{2\chi}$ term stems from the fact that these two terms are very different in nature. If we switch off the $C_{2\chi}$ term (green curves), the C_χ term also leads to an exponential grow, starting slightly before $t = \tau_s$, but it is much less important than the exponential growth from the $C_{2\chi}$ term. This is analogous to what happens for the symmetric DM case with BSF playing the role of annihilation if $C_{2\chi} = 0$.⁷ In Eq. (3) the C_χ term (linear in N_χ) is quickly counter-balanced by formation of bound-states from the A_{bsf} term (quadratic in N_χ): after a short period of exponential growth, $N_\chi \sim C_\star(e^{C_\chi t} - 1)/C_\chi$, the green curve ($C_{2\chi} = 0$), goes to a plateau from an equilibration of capture and BSF. In contrast, if $C_{2\chi} \neq 0$, the capture rate on bound-state grows as $N_{2\chi}$. Thus, due to capture on bound-state term $C_{2\chi}$, if it were not for the geometric rate upper floor, both N_χ and $N_{2\chi}$ would grow forever. Moreover, the argument of the exponential from the $C_{2\chi}$ term is larger than the one from the C_χ term, because $C_{2\chi}$ is about a factor of two times C_χ , see Fig. 2.

In presence of both C_χ and $C_{2\chi}$ terms, the C_χ term has only a moderate impact on the evolution of N_χ and $N_{2\chi}$. As a comparison of the full evolution (red curves in Fig. 3) and the $C_\chi = 0$ evolution (blue curves) shows, including C_χ reduces the timescale when the exponential growth starts, from $t \sim \tau_0$ to $t \sim \tau_s$. Thus, due to the C_χ term, the exponential effect of the $C_{2\chi}$ term starts somewhat earlier, and the geometric rate within the bound-state thermal sphere is also reached somewhat earlier. The values of N_χ and $N_{2\chi}$ are insensitive to the C_χ term at $t \gg \tau_s$.

⁷ In the limit of $C_{2\chi} \rightarrow 0$ and $A_{\text{bsf}} = 0$ (and with an additional DM annihilation term), the solution has an analytical form, first presented in [62].

III. NEUTRINO FLUX AND TERRESTRIAL DETECTION

As explained above, thanks to the capture on DMBS, the capture rate will saturate the geometric rate within the DMBS thermal sphere, leading to an equilibrium between the capture and the BSF processes. The time τ_g , at which this happens, can be easily shorter than the age of the Sun, as solved in Eqs. (A10) and (A11). At this point, the flux of mediators emitted from BSF becomes constant and is approximately given by Eq. (18) above.

For concreteness (and other reasons explained below) we will assume in the following that the mediator decays dominantly into a pair of neutrinos. Under the assumption that the mediator mass is much smaller than the binding energy, E_{bind} , the differential flux at a terrestrial detector is

$$\frac{d^2\Phi_\nu}{dE_\nu d\Omega} = \frac{A_{\text{bsf}} N_\chi^2(t_\odot)}{2\Delta\Omega} \frac{dN_\nu}{dE_\nu} = \frac{A_{\text{bsf}} N_\chi^2(t_\odot)}{8\pi d_\odot^2 (1 - \cos\vartheta)} \frac{dN_\nu}{dE_\nu}, \quad (19)$$

where d_\odot is the Earth-Sun distance (AU), with ϑ being the angular sensitivity of detector (as the apparent angular diameter of the Sun $\vartheta_\odot \approx 0.5^\circ$). Since the light mediator is boosted, the neutrino energy spectrum this decay leads to is not monochromatic but has a characteristic box shape [63]

$$\frac{dN_\nu}{dE_\nu} \simeq \frac{2}{E_{\text{bind}}} \quad \text{for } E_- \leq E_\nu \leq E_+, \quad \text{with} \quad E_\pm = \frac{E_{\text{bind}}}{2} \left(1 \pm \sqrt{1 - \frac{4m_\phi^2}{E_{\text{bind}}^2}} \right). \quad (20)$$

In particular, $E_- \simeq 0$ and $E_+ \simeq E_{\text{bind}}$ if $m_\phi \ll E_{\text{bind}}$. The differential flux of neutrinos at the detector (ignoring oscillations) is

$$\frac{d\Phi_\nu}{dE_\nu} = \frac{1}{4\pi d_\odot^2} \Gamma(m_\chi, m_\phi, \alpha_\chi, s_\theta) \frac{2}{E_{\text{bind}}} \Theta(E_+ - E_\nu) \Theta(E_\nu - E_-). \quad (21)$$

The resulting neutrino fluxes are shown in Fig. 4 for a fixed Higgs mixing angle $\sin\theta_\phi = 10^{-12}$, for $\alpha = 0.05, 0.1$ and 0.15 (in blue, red and maroon colors), respectively. For comparison, the current limits (90% C.L.) on diffuse supernova ν_e neutrino background (DSNB) flux from Super-K runs III, IV and KamLAND are shown in blue, red and black points [64–66]. Also shown are predicted atmospheric fluxes of ν_e down to 10 MeV in thin green line, assuming 30° angular resolution in the sky, adapted from [67–69]. Current measurements of atmospheric neutrino fluxes are shown in green points [70]. As this figure suggests, the neutrino flux induced by BSF could be observable. When the geometric limit for DMBS sphere is reached, the emitted flux of mediators is proportional to $C_{2\chi}^g \propto m_\chi^{-2}$. This scaling is seen in Fig. 4. If the geometric limit is not reached, heavier mediators would lead to smaller self-capture rates, as shown by the falling tails of the neutrino flux.

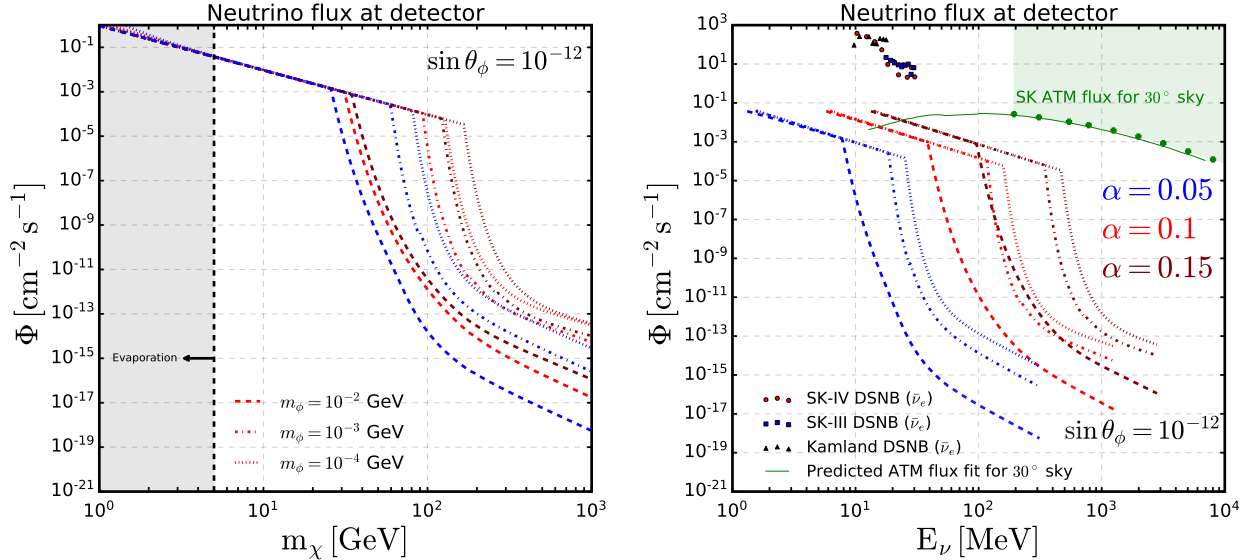


FIG. 4. *Left*: Flux of light mediators emitted by the BSF process for various parameter choices. *Right*: Neutrino flux as a function of neutrino energy, coming from the Sun for a detector placed on the surface of the Earth. Shown in red, blue and black scattered points are the current limits on diffuse supernova neutrinos adapted from [65]. Atmospheric low energy neutrino measurements from Super-K are shown by the green dots [64]. Thin green line denotes the predicted atmospheric neutrino flux for 30° sky [69].

Finally, note that our results can be easily generalized, e.g. if the mediator decays electromagnetically. Nevertheless, the experimental constraints, as studied below, also become more stringent for electromagnetic decays, further narrowing down allowed regions of parameter space.

IV. RESULTS AND CONSTRAINTS FOR AN EXPLICIT MODEL

A. Model

As mentioned above, we consider DM in the form of a (vector-like) Dirac fermion self-interacting through the exchange of a light scalar. Concretely the Lagrangian is (see e.g. [71–73])

$$\mathcal{L} \supset \mathcal{L}_{\text{SM}} + \mathcal{L}_{N_R} + \bar{\chi} (i\not{\partial} - m_\chi) \chi + \frac{1}{2} (\partial\phi)^2 - g_s \phi \bar{\chi} \chi - V(\phi, H). \quad (22)$$

Here we do not specify the scalar potential $V(\phi, H)$, and simply assume that it induces a ϕ - H mixing angle θ_ϕ (which can be achieved in various ways), so that, upon rotation to the mass basis, the following interactions are obtained:

$$\mathcal{L}_{\text{int}} = g_s \cos \theta_\phi \phi' \bar{\chi} \chi + g_s \sin \theta_\phi h' \bar{\chi} \chi + (\cos \theta_\phi h' + \sin \theta_\phi \phi') \frac{m_f}{v_H} \bar{f}_L f_R. \quad (23)$$

If we assume that neutrino masses are generated through the usual type-I seesaw mechanism, nothing prevents the right-handed neutrinos to couple in pairs to the light mediator ϕ . Thus one has the extra interactions

$$-\mathcal{L}_{N_R} = Y_\nu \bar{N} L \cdot H + \frac{m_N}{2} \bar{N}^c N + Y_\phi \phi \bar{N}^c N + \text{h.c.} . \quad (24)$$

In the physical ν' , N' and ϕ' , h' mass eigenstate basis, this leads to the following relevant Yukawa interactions for the light scalar eigenstate ϕ' , up to second order in the neutrino mixing angle,

$$\begin{aligned} -\mathcal{L}_{N_R} \supset & Y_\phi \phi' \cos \theta_\phi (\bar{N}'^c N' \cos^2 \theta_\nu + \bar{N}'^c \nu'^c \sin \theta_\nu + \bar{\nu}' N' \sin \theta_\nu + \bar{\nu}' \nu'^c \sin^2 \theta_\nu) + \text{h.c.} \\ & - Y_\nu \phi' \sin \theta_\phi (\bar{N}' \nu' \cos^2 \theta_\nu + \bar{\nu}'^c \nu' \sin \theta_\nu - \bar{N}' N'^c \sin \theta_\nu - \bar{\nu}'^c N'^c \sin^2 \theta_\nu) + \text{h.c.} . \end{aligned} \quad (25)$$

Thus, both the Y_ϕ and Y_ν interactions induce a decay of the light mediator into a pair of light neutrinos. In practice the decay induced by Y_ϕ will be dominant because various constraints require $Y_\nu \sin \theta_\phi \ll Y_\phi \sin \theta_\nu$. In the following, for simplicity, we will consider only one left-handed neutrino and one right-handed Majorana neutrino, with the neutrino mixing angle $\sin \theta_\nu \approx Y_\nu v_h / \sqrt{2} M_N$. Likewise for the associated Yukawa coupling, the typical seesaw gives

$$\sin^2 \theta_\nu \sim \frac{m_\nu}{m_N} = 10^{-13} \cdot \frac{m_\nu}{0.1 \text{eV}} \cdot \frac{1 \text{TeV}}{m_N} \quad (26)$$

with $Y_\nu \sim \sqrt{2 m_\nu m_N} / v_h^2$.

If $m_N > m_\phi$ the light mediator cannot decay into NN or $N\nu$ and the $\nu\nu$ is the only possible channel induced by the seesaw interactions. The decay width is

$$\Gamma(\phi \rightarrow \nu\nu) = \frac{1}{16\pi} |Y_\phi|^2 m_\phi \sin^4 \theta_\nu . \quad (27)$$

In addition to this neutrino-mixing channel, ϕ can also decay, through the ϕ - H scalar mixing, into pairs of charged leptons or quarks (or SM bosons for large ϕ mass). As will be discussed below, this needs to be suppressed.

B. Constraints and results

An observable neutrino flux requires sufficiently large capture and BSF rates, eventually leading to an equilibrium between both processes. This scenario must also fulfill additional phenomenological constraints:

Self-interactions: On the one hand, the corresponding self-scattering cross section is bounded from above by the observation of galaxy cluster collisions, e.g., [74–78]

$$\frac{\sigma_{\text{SI}}}{m_\chi} \lesssim 0.5 \text{ cm}^2/\text{g} , \quad (28)$$

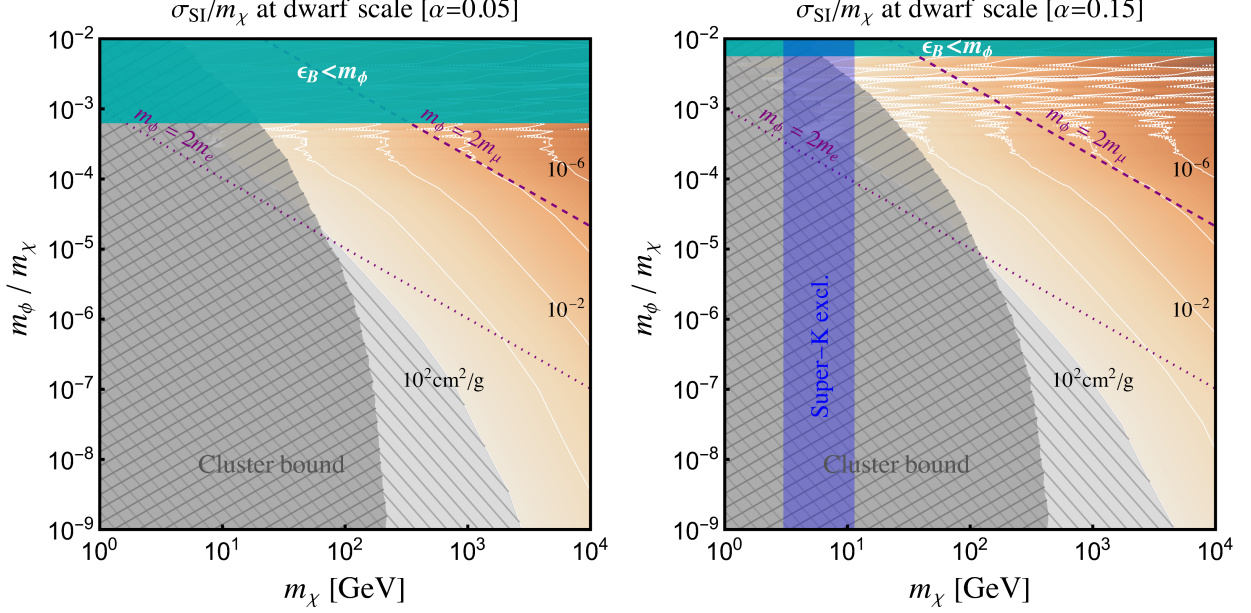


FIG. 5. Constraints for two example values of the dark coupling α . Contour lines give the values of $\sigma_{\text{SI}}/m_\chi$ in dwarf-sized halos. Black (gray) hatched regions are excluded because $\sigma_{\text{SI}}/m_\chi \geq 0.5 \text{ cm}^2/\text{g}$ at cluster scales (or $100 \text{ cm}^2/\text{g}$ at dwarfs scales, see contour lines). The resonant regime (with peaks) will become smaller in the Milky Way halo, where the average DM velocity is much larger than that at dwarfs scale.

for DM velocities around $v \sim 1000 \text{ km/s}$. On the other hand, the non-observation of gravothermal collapse in dwarf-sized halos sets an upper bound of about $100 \text{ cm}^2/\text{g}$ at small scales, for which we take $v \sim 25 \text{ km/s}$ [79, 80]. Concretely, we derive the bounds taking σ_{SI} equal to the viscosity cross section of DM particles. Adopting the modified transfer cross section barely changes the results, see Appendix B 1 for detailed discussions of these effective cross sections.

Fig. 5 shows the resulting values for this cross section as a function of m_χ and m_ϕ/m_χ for two values of α . The cluster bound excludes χ masses below ~ 10 - 1000 GeV depending on m_ϕ/m_χ and α . This figure also shows the region where m_ϕ is larger than the binding energy where BSF is not possible. Values of the cross section that could address the small scale anomalies are allowed, i.e. $\sigma_{\text{SI}}/m_\chi \in [1, 100] \text{ cm}^2/\text{g}$ at typical DM velocities of the order of 25 km/s in dwarf galaxies [81–84]. In the m_χ - α plane, Fig. 6 (right) shows the corresponding upper bound on α .

BBN: In order to observe the neutrino flux in the detector, the in-flight lifetime of the mediator must be smaller than eight minutes. This constraint is typically less stringent than that resulting from upper bounds on extra radiation after neutrino decoupling, which requires its lifetime to be shorter than one second. Using the typical seesaw expectation of Eq. (26), one gets

$$|Y_\phi|^2 \sim 0.03 \frac{100 \text{ MeV}}{m_\phi} \frac{1 \text{ s}}{\tau_\phi} \left(\frac{0.1 \text{ eV}}{m_\nu} \frac{m_N}{1 \text{ GeV}} \right)^2. \quad (29)$$

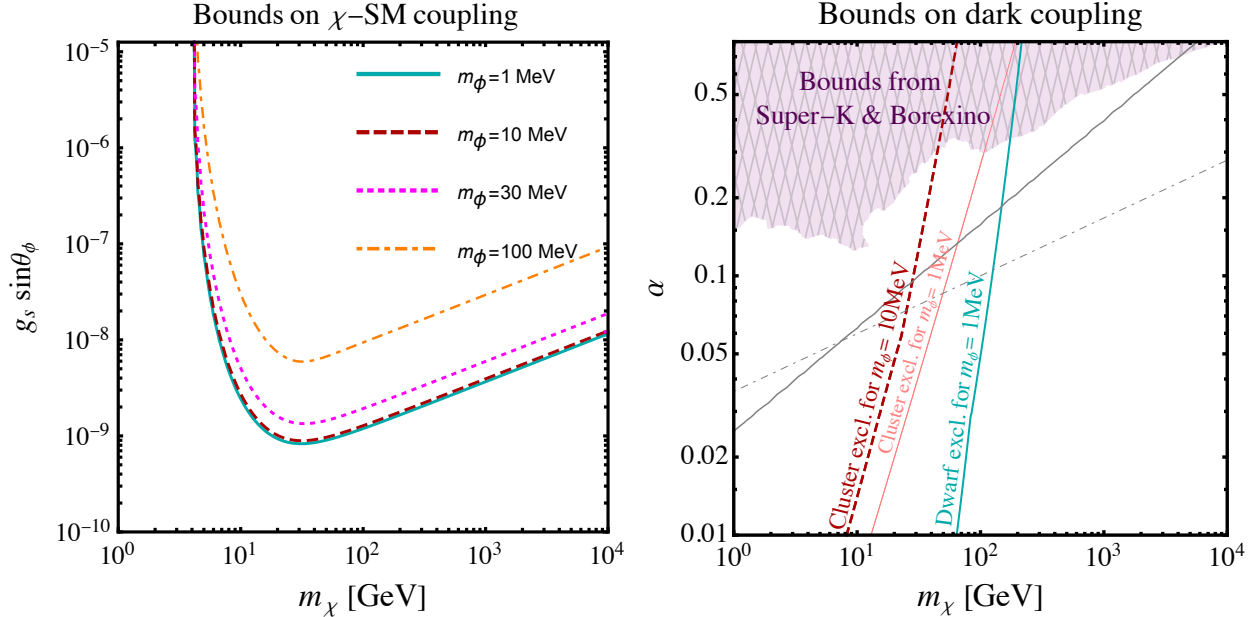


FIG. 6. *Left*: Upper bounds on the DM-SM interaction strength from XENON1T [85], depending on m_ϕ . *Right*: Upper bounds on DM coupling α from indirect search for neutrino flux (purple shaded area) and DM self-scattering at dwarfs scales. The bounds from the Bullet cluster, Eq. (28), are given for $m_\phi = 1$ MeV and 10 MeV. The conservative dwarf scale upper bound, $\sigma_{\text{SI}}/m_\chi \lesssim 100 \text{ cm}^2/\text{g}$ is given for $m_\phi = 1$ MeV. This case is disfavored by BBN observables, given its sizeable coupling to neutrinos. For $m_\phi = 100$ MeV, the dwarf galaxy scale bound is weaker and basically irrelevant for BSF. For α above the gray solid line, one expects a galactic flux from BSF in the galactic halo larger than the flux from BSF in the Sun. Efficient BSF in the early Universe is possible for parameters above the dot-dashed gray line [49].

Thus a fast enough decay is obtained provided that Y_ϕ is not too small and m_N is not too large. BBN and perturbative couplings, $Y_\phi^2 \lesssim 4\pi$, require $m_N \lesssim 20 \text{ GeV} \cdot (m_\nu/0.1 \text{ eV}) \cdot (m_\phi/100 \text{ MeV})^{1/2}$. Thus low scale seesaw is favored along this scenario. This BBN bound can be relaxed if the ϕ number density gets suppressed before neutrino decoupling.

Direct detection: As already mentioned above, due to evaporation, DM masses below a few GeV are not relevant for our purpose. Thus, non-observation of spin-independent nucleon recoil signals provides the best direct-detection bounds. For purely scalar-mediated interactions, the differential elastic scattering cross section with nuclei has been given by Eq. (11). If $m_\phi \lesssim \sqrt{2m_N E_R} \lesssim 1 \text{ MeV}$ for typical keV-scale recoil energies, direct detection rates, albeit in the Born regime, are boosted due to t -channel exchange of the light mediator, leading to more stringent bounds than for heavier mediators. The corresponding measurements by the Xenon1T experiment [85, 86] set an upper bound on $g_s \sin \theta_\phi$, which we show in Fig. 6 (left) for different masses of mediator and DM. This

obviously translates into an upper bound on the capture rate on nucleons, as both processes involve the same DM-nucleon cross section. Recent LZ data can improve the limit on $g_s \sin \theta_\phi$ by a factor of 2–3, depending on the mediator mass [87].

Indirect detection from galactic center emission: If DM BSF occurs in the Sun, it is reasonable to anticipate its occurrence in the galactic center of the Milky Way as well. Consequently, we would expect corresponding emission of energetic neutrinos originating from the galactic center, also with a box-shaped energy spectrum. Here we estimate the indirect search limit by re-scaling the current bounds on symmetric DM from neutrino telescope observations. Regarding indirect signals, a BSF process that generates one mediator and eventually two neutrinos with $E_\nu \approx E_{\text{bind}}/2$ is equivalent to symmetric DM annihilation with a mass of $E_{\text{bind}}/2$, if the latter only makes up a fraction of the observed DM abundance. Therefore, existing bounds can be rescaled as follows,

$$(\sigma_{\text{symm.}v})|_{m_\chi \rightarrow E_{\text{bind}}/2} \rightarrow \left(\frac{E_{\text{bind}}/2}{m_\chi}\right)^2 (\sigma_{\text{BSF}v}), \quad (30)$$

where $(\sigma_{\text{symm.}v})$ denotes the known bounds on symmetric DM as a function of the DM mass.

Quantitatively, the neutrino flux generated from the BSF process of halo DM particles is estimated to be

$$\Phi_\nu^{\text{D}} \sim 1 \text{ cm}^{-2} \text{ s}^{-1} \left(\frac{\text{GeV}}{m_\chi}\right)^2 \left(\frac{\sigma_{\text{BSF}v}}{3 \times 10^{-22} \text{ cm}^3/\text{s}}\right). \quad (31)$$

This is similar to boosted DM case [88], which can vary mildly due to the uncertainty of the Galactic J-factor [89]. The corresponding upper bound on α is shown in the right panel of Fig. 6, obtained from re-scaling the indirect bounds holding in the symmetric DM case [90]. As also illustrated in Fig. 5, this excludes values of m_χ between 3.0 and 11.4 GeV for $\alpha = 0.15$, and gives irrelevant bound for $\alpha = 0.05$.

We can further speculate when this galactic neutrino flux is larger than the one induced by BSF inside the Sun. The latter is approximately $\Phi_\nu^\odot / (\text{GeV}/m_\chi)^2 \sim \mathcal{O}(1) \text{ cm}^{-2} \text{ s}^{-1}$ when the DM capture on DMBS is saturated by its geometric rate. Using Eq. (12) results in $\alpha^{5/2}/m_\chi \lesssim 10^{-4}/\text{GeV}$, which in turn requires $m_\chi \gtrsim 5.6 \text{ GeV}$ (87.1 GeV) for $\alpha = 0.05$ (0.15), see also the right panel of Fig. 6. In practice, the non-vanishing mass of the mediator suppresses the BSF cross section, reducing the neutrino flux, but barely affects the BSF-induced flux from the Sun.

CMB: Since the CMB observables are mostly sensitive to the total electromagnetic energy injected by extra processes in the high-redshift Universe, the associated constraint on BSF can be obtained by re-scaling the CMB bound on the annihilation of a symmetric DM candidate [91],

$$f_{\text{eff}} \frac{\sigma_{\text{BSF}v}}{m_\chi} \frac{\text{Br}_{\phi \rightarrow \text{EM}} E_{\text{bind}}}{2m_\chi} \lesssim 4.1 \times 10^{-28} \frac{\text{cm}^3/\text{s}}{\text{GeV}}. \quad (32)$$

Here, f_{eff} is an efficiency factor that depends on the spectrum of injected electrons and photons, and we have taken into account that the energy injected per process is not about $2m_\chi$ as in the case of DM annihilation, but is given by the binding energy $\approx \alpha^2 m_\chi/4$, times the electromagnetic branching ratio of ϕ decay, $\text{Br}_{\phi \rightarrow \text{EM}}$. For $m_\phi \ll E_{\text{bind}}$, the mass of the light mediator does not play any role in the CMB bound. For decay into SM particles other than neutrinos, the fact that BSF is strongly enhanced when the DM relative velocity is small gives a CMB bound which is much stronger than other bounds derived from local cosmic-ray observations such as Fermi-Lat and AMS experiments. For instance, taking the DM velocity at CMB to be a few km/s leads to $\text{Br}_{\phi \rightarrow \text{EM}}^{1/3} \alpha^{7/3} \lesssim 10^{-5} m_\chi/\text{GeV}$. Combining this condition with Eq. (27) gives the constraint $Y_\phi \theta_\nu^2/\theta_\phi \gtrsim 10^{2.2} \alpha^{7/2} (\text{GeV}/m_\chi)^{3/2}$ for m_ϕ below twice the muon mass. For typical seesaw values of the neutrino mixing angle, Eq. (26), this translates to the condition $m_N \lesssim 22 \text{ TeV} \cdot Y_\phi (m_\chi/5 \text{ GeV})^{3/2} (10^{-12}/\theta_\phi) (0.1/\alpha)^{7/2} (m_\nu/0.1 \text{ eV})$.

Mediator decay into right-handed neutrinos: If $2m_N < m_\phi$ the dominant decay is not anymore into a pair of light neutrinos but into a pair of right-handed neutrinos (or into νN for $m_\phi/2 < m_N < m_\phi$), with their decay widths given by,

$$\Gamma(\phi \rightarrow NN) = \frac{1}{16\pi} |Y_\phi|^2 m_\phi, \quad \Gamma(\phi \rightarrow N\nu) = \frac{1}{16\pi} |Y_\phi|^2 m_\phi \sin^2 \theta_\nu. \quad (33)$$

Using the typical seesaw expectation of Eq. (26), one gets

$$|Y_\phi|^2 \sim 10^{-22} \frac{1 \text{ GeV}}{m_\phi} \frac{1 \text{ s}}{\tau_\phi}, \quad |Y_\phi|^2 \sim 10^{-12} \frac{1 \text{ GeV}}{m_\phi} \frac{1 \text{ s}}{\tau_\phi} \frac{0.1 \text{ eV}}{m_\nu} \frac{m_N}{1 \text{ GeV}} \quad (34)$$

for $2m_N < m_\phi$ and $m_\phi/2 < m_N < m_\phi$, respectively. This can be compatible with the extra radiation constraint $\tau_\phi \lesssim 1 \text{ s}$ but is basically excluded by the CMB bound because the right-handed neutrino decay product contains a non-negligible amount of electromagnetic material.

V. SUMMARY

We have considered the possibility that asymmetric DM forms bound-states in the Sun, and showed that this leads to novel phenomenology. BSF in the Sun can proceed via emission of light scalar particles that carry energy roughly equal to the binding energy. Their decays to neutrinos lead to potentially testable low energy signals at neutrino detectors.

Unlike for annihilating DM, BSF produces a flux of particles without reducing the number of DM particles in the Sun. We point out that on top of the DM particles captured in the Sun, the bound-states piling up in this way become additional scattering targets through which DM from

the galactic halo could be captured. We have determined the associated DM accretion rates on DM and DM bound-states by evaluating the differential cross section, taking into account that for typical parameters, $v \sim 10^{-3}$, $\alpha \sim 0.1$, $m_\phi < \text{GeV}$ and $m_\chi \sim 100 \text{ GeV}$, the DM-DM and DM-DMBS scattering processes proceed in the semi-classical regime. As soon as these self capture rates are larger than t_\odot^{-1} , they can become phenomenologically relevant. In particular, we have shown that, thanks to the self-capture on bound-states, the number of DM particles in the Sun can exponentially increase, so much that the capture rate can reach the geometric rate, i.e. all the DM particles intercepting the DM bound-state thermal sphere are captured as the mean free path becomes smaller than the sphere. As a result, this exponential effect also considerably boosts the BSF and thus the associated flux of light mediators. In an example model, where DM is a Dirac fermion which self-interacts through exchange of light scalar that mixes with the Higgs boson, with the scalar decaying into two neutrinos through seesaw interactions, this leads to a neutrino flux which reach the predicted atmospheric neutrino fluxes at energies below hundred MeV. Near future experiments such as Hyper-K, as well as direct detection experiments, will be able to probe further this scenario.

Acknowledgments: We thank Sergio Palomares-Ruiz and Hai-bo Yu for discussions, and Sebastian Wild for help with the implementation of direct detection rates in DDCalc [86]. X.C. is supported by the Research Network Quantum Aspects of Spacetime (TURIS) and co-funded by the European Union (ERC, NLO-DM, 101044443). R.G. is supported by MIUR grants PRIN 2017FMJFMW and 2017L5W2PT, and thanks Galileo Galilei Institute for hospitality. C.G.C. is supported by a Ramón y Cajal contract with Ref. RYC2020-029248-I, the Spanish National Grant PID2022-137268NA-C55 and Generalitat Valenciana through the grant CIPROM/22/69. The work of T.H. is supported by the Excellence of Science (EoS) project No. 30820817 - be.h “The H boson gateway to physics beyond the Standard Model”, by the IISN convention 4.4503.15, and by CERN where part of this work has been done. The authors acknowledge the workshop on Self-Interacting Dark Matter: Models, Simulations and Signals 2023, Pollica, for hospitality.

Appendix A: Approximate parametric solution to number evolution of DM particles

The set of coupled Boltzmann equations for N_χ and $N_{2\chi}$, Eqs. (2)-(3), has no closed-form analytical solution. However, we can construct an approximate solution and better understand the underlying physics by proceeding step by step as follows.

1. Case with no self-capture on DM bound-states

Without the $C_{2\chi}$ term, the equation for N_χ does not depend on $N_{2\chi}$

$$\frac{dN_\chi}{dt} = C_\star - A_{\text{bsf}}N_\chi^2 + C_\chi N_\chi, \quad (\text{A1})$$

which can be solved easily as follows.

BSF with capture only on nucleons: $C_\chi = C_{2\chi} = 0$: Without any capture due to DM self-interactions, the above equation has the solution

$$N_\chi^0(t) = C_\star \tau_0 \tanh\left(\frac{t}{\tau_0}\right), \quad N_{2\chi}^0(t) = \frac{1}{2}C_\star \left(t - \tau_0 \tanh\left(\frac{t}{\tau_0}\right)\right), \quad (\text{A2})$$

with the time constant given by $\tau_0 = (C_\star A_{\text{bsf}})^{-1/2}$. Without BSF, i.e. when $\tau_0 \rightarrow \infty$, this solution gives a N_χ linearly increasing in time as expected, $N_\chi^0(t \lesssim \tau_0) = C_\star t$. With BSF, such an increase occurs until there are enough DM particles for BSF to proceed. For $t \gtrsim \tau_0$, an equilibrium between BSF and capture on nucleons is reached so that N_χ saturates becoming constant: $N_\chi = C_\star \tau_0 = (C_\star/A_{\text{bsf}})^{1/2}$. This value can be obtained also directly from the Boltzmann equation, Eq. (2), whose right-hand side vanishes when $C_\star - A_{\text{bsf}}N_\chi^2 = 0$. As expected, the larger A_{bsf} , the sooner the saturation is reached and the smaller the asymptotic value of N_χ is. Conversely, the larger C_\star , the larger N_χ must be for the term associated with BSF to compensate that of C_\star . Note, nevertheless, that the larger C_\star and the larger A_{bsf} , the smaller the saturation time scale τ_0 . This stems from the fact that the number of particles captured increases more rapidly, and BSF starts to become important earlier. Consequently, BSF catches up with the capture process sooner.

BSF with capture on nucleons and on free DM particles: $C_\chi \neq 0, C_{2\chi} = 0$: Early in the evolution the contribution of $C_{2\chi}N_{2\chi}$ is negligible. The analytical solution when $C_{2\chi} = 0$ and $C_\chi \neq 0$ is

$$N_\chi^s(t) = \frac{C_\chi}{2A_{\text{bsf}}} + \frac{1}{A_{\text{bsf}}\tau_s} \tanh\left(\frac{t}{\tau_s} - \text{arctanh}\left(\frac{C_\chi\tau_s}{2}\right)\right), \quad (\text{A3})$$

$$2N_{2\chi}^s(t) + N_\chi^s(t) = \left(C_\star + \frac{C_\chi^2}{2A_{\text{bsf}}} + \frac{C_\chi}{A_{\text{bsf}}\tau_s}\right)t + \frac{C_\chi}{A_{\text{bsf}}} \log\left(\frac{2 - C_\chi\tau_s + e^{-\frac{2t}{\tau_s}}(2 + C_\chi\tau_s)}{4}\right) \quad (\text{A4})$$

with $\tau_s = (C_\star A_{\text{bsf}} + C_\chi^2/4)^{-1/2}$. As it must be, for $C_\chi = 0$ these equations reduce to Eq. (A2) and τ_s reduces to τ_0 .

Here again, the BSF term equilibrates with capture in Eq. (2), as it is negative and quadratic in N_χ , whereas the C_\star (C_χ) term is constant (linear) in it. Thus, N_χ saturates when the right-hand side of Eq. (2) vanishes, $C_\star - A_{\text{bsf}}N_\chi^2 + C_\chi N_\chi = 0$, which gives $N_\chi^{s,\text{eq}} = C_\chi/(2A_{\text{bsf}}) + 1/(\tau_s A_{\text{bsf}}) =$

$C_\star/(\tau_s^{-1} - C_\chi/2)$. The equilibrium time scale τ_s is smaller than that without the C_χ term, τ_0 , because the C_χ term increases the capture, so that BSF becomes important earlier. Note that before equilibrium is reached the solution of Eq. (A3) is exponential. However the effect of this exponential is very limited as the equilibrium is reached soon, as can be seen in Fig. (3), for various examples of parameter sets.⁸ Note also that the total number of particles grows linearly, Eq. (A4), except for a logarithmic correction, particularly for $t \gg \tau_s$. More importantly, for realistic values of C_\star and C_χ , the rate associated with the saturation value always lies well below the geometric rate C_χ^g of thermalized DM particles in the Sun.

2. Case with self-capture on DM bound-states

The appearance of a non-vanishing $C_{2\chi}$ term drastically changes the physics in several ways. First of all, the $C_{2\chi}$ term implies that the number of free DM particles in the Sun depends on the number of DM bound-states so that the Boltzmann equations for N_χ and $N_{2\chi}$ are coupled. Differentiating Eq. (2) with respect to time and using the equation for the bound-state, Eq. (3), results in the following second-order differential equation,

$$\frac{d^2 N_\chi}{dt^2} = (-2A_{\text{bsf}}N_\chi + C_\chi) \frac{dN_\chi}{dt} + \frac{1}{2}C_{2\chi}A_{\text{bsf}}N_\chi^2, \quad (\text{A5})$$

with boundary conditions: $\frac{dN_\chi(t=0)}{dt} = C_\star$ and $N_\chi(t=0) = 0$. Formally, Eq. (A5) is of the form $N'' = f(N)N' + g(N)$, known as a Liénard equation, with no known general analytical solutions.

Second, the self-capture associated with $C_{2\chi}$ is larger than that induced by C_χ . This and the fact that $N_{2\chi}$ never saturates –as Eq. (3) shows– imply that the term $C_{2\chi}N_{2\chi}$ in Eq. (2) becomes much larger than $C_\chi N_\chi$. In fact, N_χ saturates to values much larger than in the case of $C_\chi \neq 0, C_{2\chi} = 0$, because the right-hand side of Eq. (2) vanishes for $A_{\text{bsf}}N_\chi^2 \simeq C_{2\chi}N_{2\chi} \gg C_\chi N_\chi$. Thus, unlike in the case of $C_\chi \neq 0, C_{2\chi} = 0$, where the exponential growth induced by the C_χ term does not last long, the $C_{2\chi}$ term induces an exponential growth for N_χ which is both faster (since the argument of the exponential will be proportional to $C_{2\chi}$ rather than to C_χ) and much larger. Therefore, N_χ can reach in this way much higher values, large enough for the capture rate to reach the geometric limit within the DMBS thermal sphere. Approximate solutions can be obtained as follows.

⁸ Actually the solution of Eq. (A3) can be rewritten in exponential form as $2C_\star\tau_s(e^{2t/\tau_s} - 1)/(A + Be^{2t/\tau_s})$ with $A = -2 - C_\chi\tau_s$ and $B = -2 + C_\chi\tau_s$. In practice if $C_\star A_{\text{bsf}} < C_\chi^2/4$ (as will be the case for our scenario), then $\tau_s \simeq 2/C_\chi$ which gives $B < A$ so that $N_\chi \simeq 2C_\star\tau_s(e^{2t/\tau_s} - 1)/A$, which is exponentially growing until it reaches the equilibrium plateau when Be^{2t/τ_s} becomes larger than A . The amount of exponential grows is limited because in practice B is not much smaller than A .

BSF with capture on nucleons and on DM bound-states: $C_\chi = 0, C_{2\chi} \neq 0$: For the parameters of interest in this work, $C_{2\chi} \ll 100/\tau_0$, we numerically find that the following exponential ansatz provides a good approximation from $t = \tau_0$ to the point when $C_{2\chi}N_{2\chi}$ saturates the geometric capture rate. That is, in practice

$$N_\chi(\tau_0 \lesssim t \lesssim \tau_g) = N_\chi^0(\tau_0) \exp \left[\frac{C_{2\chi}}{4}(t - \tau_0) \right]. \quad (\text{A6})$$

This is also suggested by the quasi-static solution of $dN_\chi/dt \sim 0$ in Eqs. (2) and (3), where

$$\frac{dN_{2\chi}}{dt} \simeq \frac{C_\star}{2} + \frac{C_{2\chi}}{2}N_{2\chi} \quad \text{and} \quad N_\chi \simeq \left(\frac{C_\star + C_{2\chi}N_{2\chi}}{A_{\text{bsf}}} \right)^{1/2}. \quad (\text{A7})$$

For the opposite case, $C_{2\chi} \geq 100/\tau_0$, the divergence happens even faster.

Therefore, capture on bound-states exponentially increases the number of DM particles within the Solar lifetime if the condition, $t_\odot - \tau_0 \gg C_{2\chi}^{-1}$ is satisfied. The fact that the exponential growth starts when $N_{2\chi}$ becomes of order N_χ can also be seen in the numerical examples shown in Fig. 3.

BSF in the full general case: $C_\chi \neq 0, C_{2\chi} \neq 0$: For the reasons explained above, switching on the C_χ term –in addition to the $C_{2\chi}$ term– does not drastically change the result. It induces an additional moderate exponential growth that makes the contribution of $C_{2\chi}$ important slightly earlier (i.e. around $t = \tau_s$ rather than at τ_0), see Fig. 3. An approximate solution to this general case is obtained in the same way as Eq. (A6), by matching Eq. (A3) at τ_s rather than at τ_0 . Interestingly, since $\tau_s < 2/C_\chi \sim 4/C_{2\chi}$, we have $\tau_s C_{2\chi} \lesssim 4$. That is, the condition for the validity of Eq. (A6), $C_{2\chi} \ll 100/\tau_0$, in which τ_0 is now replaced by τ_s , is automatically satisfied. This suggests

$$N_\chi(\tau_s \lesssim t \lesssim \tau_g) = N_\chi^s(\tau_s) \exp \left[\frac{C_{2\chi}}{4}(t - \tau_s) \right], \quad (\text{A8})$$

where $N_\chi^s(\tau_s)$ is well approximated by Eq. (A3).

This exponential growth lasts until the geometric capture rate within the DMBS thermal sphere is saturated. Quickly after $t = \tau_g$, N_χ stops increasing when the BSF term (quadratic in N_χ) compensates the constant capture rate.⁹ The quasi-static equilibrium solution, obtained from $dN_\chi/dt \simeq C_\star + C_{2\chi}^g - A_{\text{bsf}}N_\chi^2 \simeq 0$, yields the final particle number¹⁰

$$N_\chi(t > \tau_g) = \left(\frac{C_{2\chi}^g + C_\star}{A_{\text{bsf}}} \right)^{1/2}. \quad (\text{A9})$$

⁹ Once the capture rate reaches the DMBS sphere geometric rate, the time it takes for N_χ to become constant is small, $\Delta t \simeq 1/\sqrt{A_{\text{bsf}}C_{2\chi}^g}$.

¹⁰ Here we neglect the subleading capture contribution, from the C_χ term, within the DM thermal sphere outside the DMBS thermal sphere. To be accurate the C_\star term in Eq. (A9) has to be taken into account only outside the DMBS thermal sphere as the $C_{2\chi}^g$ term already accounts for the maximal total capture rate within this sphere, but this concerns a negligible effect.

The associated time τ_g , where such an equilibrium is reached, is determined as

$$\tau_g = \tau_s + \frac{2}{C_{2\chi}} \log \left(\frac{C_{2\chi}^g + C_\star}{A_{\text{bsf}}(N_\chi^s(\tau_s))^2} \right). \quad (\text{A10})$$

The condition that $\tau_g \leq t_\odot$, so that the DM number can be maximized at present, is satisfied if

$$\frac{C_{2\chi}}{2} (t_\odot - \tau_s) \geq \log \left(\frac{C_{2\chi}^g + C_\star}{A_{\text{bsf}}(N_\chi^s(\tau_s))^2} \right) = \begin{cases} \log \left(\frac{C_{2\chi}^g/C_\star + 1}{\tanh[1]^2} \right) & \text{if } C_\chi^2 \leq A_{\text{bsf}}C_\star \\ \log \left(\frac{C_{2\chi}^g/C_\star + 1}{(e^2 - 1)^2} \frac{C_\chi^2}{A_{\text{bsf}}C_\star} \right) & \text{if } C_\chi^2 \gg A_{\text{bsf}}C_\star \end{cases}. \quad (\text{A11})$$

The latter case has $\tau_0 \gg \tau_s \simeq 2/C_\chi \sim 4/C_{2\chi}$, so the saturation should happen within a few τ_s .

We can now analytically match the above two solutions at times $\sim \tau_s$ and τ_g . The final approximate solution for species i has the parametric form

$$N_i(t) = N_i^{t < \tau_s} \Theta(\tau_s - t) + N_i^{\tau_s < t < \tau_g} \Theta(t - \tau_s) \Theta(\tau_g - t) + N_i^{t > \tau_g} \Theta(t - \tau_g), \quad (\text{A12})$$

where $N_i^{t < \tau_s}$, $N_i^{\tau_s < t < \tau_g}$ and $N_i^{t > \tau_g}$ are given by Eqs. (A3), (A8) and (A9), respectively. We have checked that these analytical expressions agree well with our numerical results presented in the various figures from solving the Boltzmann equations.

Appendix B: (Non-)perturbative treatment of elastic DM scattering

Suppose that DM scatters off a target with a mass m_T with a negligible form factor, the cross section differential in the recoil energy is

$$\frac{d\sigma}{dE_R} = \frac{2\pi m_T}{k^2} |\mathcal{M}(k, \theta)|^2, \quad \text{with} \quad \cos \theta = 1 - \frac{m_T E_R}{k^2}. \quad (\text{B1})$$

Here θ and $k = \mu v$ are respectively the scattering angle and the incoming momentum in the center of mass frame, while the reduced mass of the DM-target system $\mu = m_\chi m_T / (m_\chi + m_T)$. We aim to calculate this when the scattering is triggered by the exchange of a scalar mediator, particularly when non-perturbative effects cannot be disregarded. In the non-relativistic limit, this is described by a free DM particle scattered by the corresponding Yukawa potential $V(r) = -\alpha' e^{-m_\phi r} / r$, with $\alpha' = g_s y_N \sin \theta_\phi / 4\pi, \alpha$ or 2α when target is a nucleon, a DM particle or a DMBS, respectively.

The amplitude of such quantum scattering can be obtained from a partial-wave expansion

$$\mathcal{M}(k, \theta) = \frac{1}{2ik} \sum_{\ell=0}^{\infty} (2\ell + 1) P_\ell(\cos \theta) \left(e^{2i\delta_\ell} - 1 \right), \quad (\text{B2})$$

where ℓ is the orbital angular momentum, $P_\ell(\cos \theta)$ is the corresponding Legendre polynomial and δ_ℓ is the phase-shift. In general, the phase-shift must be obtained by solving the radial part of the

Schrödinger equation describing the collision, which is equivalent to solving [92]

$$\delta'_{\ell,k}(r) = -2k\mu r^2 V(r) \operatorname{Re} \left[e^{i\delta_{\ell,k}(r)} h_\ell^{(1)}(kr) \right]^2 \quad \text{with } \delta_{\ell,k}(0) = 0 \text{ and } \delta_{\ell,k}(r)|_{r \rightarrow \infty} \rightarrow \delta_\ell. \quad (\text{B3})$$

Here, $h_\ell^{(1)} = j_\ell + i n_\ell$ is the spherical Hankel function of the first kind. Nevertheless, solving Eq. (B3) for all values of ℓ is impractical, and thus simplifications are necessary for different parameter regimes, as shown in left panel of Fig. 7. This will be discussed below for integrated and differential DM-DM(BS) scattering, separately. The Born approximation is always justified for the very weak scattering between DM and nucleon.

1. Integrated DM self-scattering in DM halos

Sufficiently large DM self-scattering can alter the evolution of halos, which gives rise to constraints on the corresponding scattering rates. As argued in Ref. [93], the gravothermal evolution of such halos is best characterized by the so-called viscosity cross section, $\sigma_V \equiv \frac{3}{2} \int_{-1}^1 d \cos \theta \sin^2 \theta \frac{d\sigma}{d \cos \theta}$.¹¹ The parameter regimes where the Born and semi-classical approximations apply are given in left panel of Fig. 7.

For $\alpha \lesssim v$ or $m_\chi \lesssim m_\phi/\alpha$, the first-order Born approximation is justified [59]. Note that $\mu = m_\chi/2$ and $\alpha' = \alpha$ in this case. Moreover, accounting for the indistinguishability of the DM particles in $\chi - \chi$ scattering, we find

$$\sigma_V = \frac{6\pi\beta^2}{m_\phi^2} \left(\frac{\left(\frac{m_\chi v}{m_\phi}\right)^4 + 5 \left(\frac{m_\chi v}{m_\phi}\right)^2 + 5}{\left(\frac{m_\chi v}{m_\phi}\right)^4 + 2 \left(\frac{m_\chi v}{m_\phi}\right)^2} \log \left[\left(\frac{m_\chi v}{m_\phi}\right)^2 + 1 \right] - \frac{5}{2} \right). \quad (\text{B4})$$

Where we have introduced $\beta = 2m_\phi\alpha/(m_\chi v^2)$ for later convenience. Note that if one adopts the modified transfer cross section, defined as $\sigma_{|T|} \equiv \int_{-1}^1 d \cos \theta (1 - |\cos \theta|) \frac{d\sigma}{d \cos \theta}$, approximately $\sigma_V \simeq 2\sigma_{|T|}$ if $m_\chi v/m_\phi \ll 1$ as well as $\sigma_V \simeq 3\sigma_{|T|}$ if $m_\chi v/m_\phi \gg 1$.

Outside the Born regime, non-perturbative effects are non-negligible, especially in the resonant regime ($\alpha m_\chi/m_\phi \gtrsim 1$ and $m_\chi v/m_\phi \lesssim 1$). In spite of this, in this parameter region the scattering is generally dominated by the s -wave, $\ell = 0$ [57], for which we can adopt the analytical results obtained by solving for the phase shift, δ_0 of $\ell = 0$, under the assumption that the Yukawa potential can be approximated by a Hulthén potential [94]. For identical fermions, after adding the symmetric factor $1/2$ for final states, this leads to

$$\sigma_V = \frac{4\pi}{2} \frac{d\sigma}{d\Omega} \Big|_{\ell=0} = \frac{2\pi}{k^2} \left| e^{i\delta_0} \left(P_0(\cos \theta) + P_0(-\cos \theta) \right) \sin \delta_0 \right|^2 = \frac{8\pi}{k^2} \left| e^{i\delta_0} \sin \delta_0 \right|^2, \quad (\text{B5})$$

¹¹ Following Ref. [93], we introduce a prefactor of $3/2$ to make $\sigma_V = \sigma$ for isotropic scatterings.

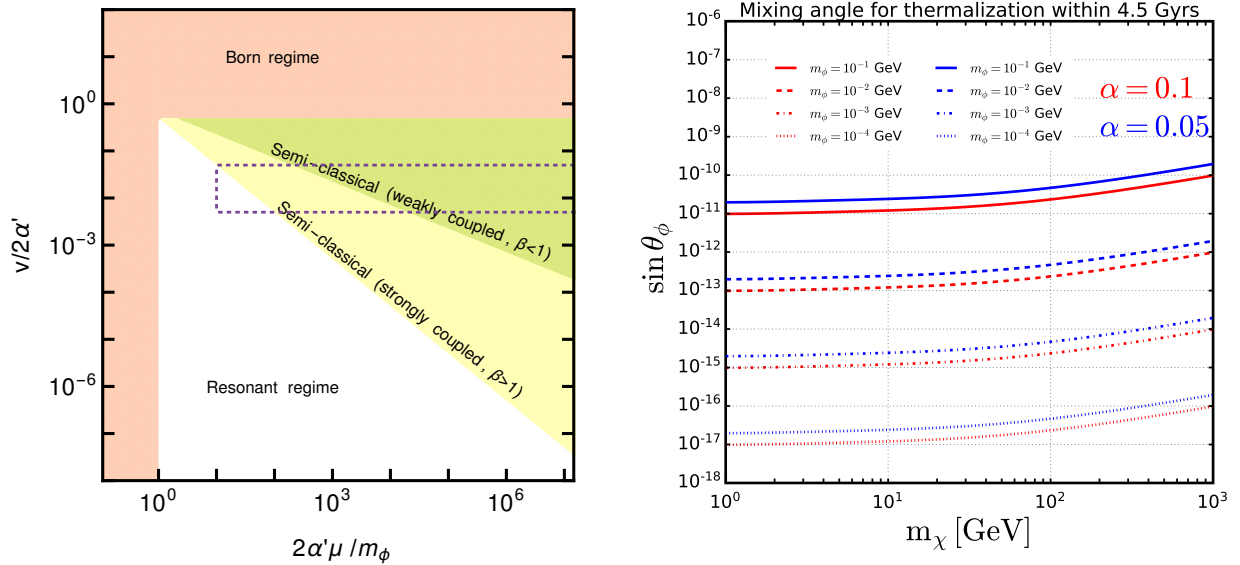


FIG. 7. *Left*: Dark matter self-scattering regimes. For self-capture of dark matter by the Sun, the relevant parameters roughly lie within the dotted line, and correspond to $v \sim 4 \cdot 10^{-3}$, $m_\chi \gtrsim 5$ GeV, 10^{-4} GeV $\lesssim m_\phi \lesssim 10^{-2}$ GeV, and $0.02 \lesssim \alpha < 0.2$. See text for details. *Right*: Curves above which the captured DM particles thermalize with the nucleons in the Sun within t_\odot .

where the scattering is isotropic, $k = m_\chi v/2$, and P_0 is the 0th-order Legendre polynomial. Note that this cross section only includes an even spatial wave-function and an anti-symmetric spin wave-function. We take the probability of such anti-parallel spin alignment to be $1/4$. That is, its corresponding cross section for identical fermion is reduced by half with respect to that of non-identical fermions. The characteristic peaks of this regime are visible in Figs. 2 and 5.

Finally, with the resulting expressions of the viscosity cross section for all regimes, we impose bounds on DM self-interaction at both cluster and dwarf scales, obtaining the observationally allowed parameter region shown in Fig. 5, see also section IV.

2. Differential DM-DM(BS) scattering for DM capture

As explained in the main text and above, while the impact of DM self-interactions in galaxies and galaxy clusters can be characterized by the integrated transfer or viscosity total cross sections, for DM self-capture in the Sun, it is crucial to obtain the differential scattering cross section. In the latter case, left panel of Fig. 7 (dotted contour) illustrates the parameter region of interest for the DM capture via scatterings off free and bound DM particles already captured in the Sun.

The relevant parameters largely lie in the semi-classical regime, where $k \gg m_\phi^{-1}$. That is, the

de Broglie wavelength is much larger than the range of the Yukawa potential and the scattering amplitude can be estimated semi-classically. More precisely, the resulting sum in Eq. (B2) can be performed using the stationary phase approximation [59], which, up to an inconsequential global phase, gives

$$\mathcal{M} = \frac{1}{k} \left(\frac{\ell_0(\theta)}{\sin \theta} \left| \frac{d\ell_0(\theta)}{d\theta} \right| \right)^{\frac{1}{2}}, \quad \text{where} \quad \int_{r_0}^{\infty} \frac{\ell_0(\theta) + \frac{1}{2}}{r^2 \sqrt{k^2 - \left(\frac{\ell_0(\theta) + \frac{1}{2}}{r} \right)^2 - 2\mu V(r)}} dr = \frac{\pi + \theta}{2}. \quad (\text{B6})$$

Here r_0 is the closest distance from the potential centre, and $\ell_0(\theta)$ is the angular-momentum minimizing the phase in Eq. (B2) for a given scattering angle θ . All this applies as long as $\ell_0(\theta) \gg 1$, which justifies neglecting $1/2$ in Eq. (B6). To see how Eq. (B6) resembles the classical equations of motion, we define the impact parameter as $\rho \equiv \ell_0(\theta)/k$, which together with Eq. (B1), leads to

$$\frac{d\sigma}{d \cos \theta} = 2\pi\rho \frac{d\rho}{d \cos \theta}, \quad \text{where} \quad \int_{r_0}^{\infty} \frac{\rho dr}{r^2 \sqrt{1 - \frac{\rho^2}{r^2} + 2\beta \left(\frac{e^{-m_\phi r}}{m_\phi r} \right)}} = \frac{\pi + \theta}{2}, \quad (\text{B7})$$

with $\beta \equiv \mu m_\phi \alpha' / k^2$. The integral in Eq. (B7) gives the scattering angle according to classical mechanics. In this work, we follow the numerical approach presented in Ref. [60, 61] to solve Eq. (B7) and obtain the scattering rates.

As shown by Ref. [61], the calculation can be further simplified for $\beta > 13.2$, where the angular dependence of $d\sigma/d \cos \theta$ becomes insensitive to β . Performing a numerical fit to the cross sections of non-identical scattering and defining $d\sigma/d \cos \theta \equiv \pi \rho_*^2(\beta, m_\phi) \mathcal{N}(\cos \theta)$, we find

$$\mathcal{N}(c_\theta) \simeq 0.35 + 0.05c_\theta + 2.09c_\theta^3 + 3.25c_\theta^4 - 5.51c_\theta^5 - 8.53c_\theta^6 + 5.06c_\theta^7 + 7.22c_\theta^8. \quad (\text{B8})$$

Note that the normalization, $\int_{-1}^1 dc_\theta (1 - c_\theta) \mathcal{N}(c_\theta) \simeq 1$, is chosen in a way we can directly adopt the overall prefactor from [60] as

$$\rho_*^2(\beta, m_\phi) = \begin{cases} \frac{1}{m_\phi^2} \left(\log \beta + 1 - \frac{1}{2 \log \beta} \right)^2 & \text{for } \beta > 1000, \\ \frac{8}{m_\phi^2} \left(\frac{\beta^2}{1 + 1.5 \beta^{1.65}} \right) & \text{for } 1000 > \beta > 13.2. \end{cases} \quad (\text{B9})$$

The amplitudes at the vicinity of $\cos \theta = 1$, which may approach infinity, are not included in the numerical fit above, given that small-angle scatterings barely contribute to the self-capture rate as a result of θ_{\min} in Eqs. (15) and (16).

Besides, under the assumption that the interference is subleading in the (semi-)classical regime [95], the previous approach can also be applied to the scattering of identical particles

by symmetrizing the differential scattering amplitude $\theta \rightarrow \pi - \theta$, as

$$\left. \frac{d\sigma}{d \cos \theta} \right|_{\chi\chi} = \left. \frac{d\sigma}{d \cos \theta} \right|_{\cos \theta \rightarrow -\cos \theta} , \quad (\text{B10})$$

where the range of the scattering angle θ reduces to $[0, \pi/2]$.

Appendix C: DM thermalization

We summarize below the general formalism for DM thermalization with the Solar medium, and present the results applicable to the scenario presented in the main text. After being captured, DM particle orbits become smaller than the size of the celestial body. For contact interactions, the time taken for the orbits to shrink to its thermal radius is given by [96]

$$t_{\text{therm}} = \frac{m_\chi}{(\sum_N \rho_N \sigma_{\chi N})} \sqrt{\frac{m_\chi}{2T}} . \quad (\text{C1})$$

For the Sun, the time scale is estimated via

$$t_2^\odot = 1.5 \text{ yrs} \left(\frac{m_\chi}{10 \text{ GeV}} \right)^{3/2} \left(\frac{2.2 \text{ KeV}}{T_c} \right)^{1/2} \left(\frac{150 \text{ g/cm}^3}{\rho_c} \right) \left(\frac{10^{-40} \text{ cm}^2}{\sigma_{\chi N}} \right) . \quad (\text{C2})$$

Thermalization time is dominated by the last stages of the process with the typical energy and momentum transfer of the order of temperature [97]. Formally, thermalization time is computed through the energy loss rate. Consider the elastic scattering of a DM particle χ off a distribution of target particles T : $\chi(k) + T(p) \rightarrow \chi(k') + T(p')$. The interaction rate per DM particle reads [98, 99]:

$$d\Gamma = 2 \frac{d^3 k'}{(2\pi)^3} S(q_0, q) ,$$

$$S(q_0, q) = \iint \frac{d^3 p' d^3 p}{(2\pi)^6 2E_{p'} 2E_{k'} 2E_p 2E_k} (2\pi)^4 \delta^4(k + p - k' - p') |\mathcal{M}|^2 f(E_p) (1 - f(E_{p'})) , \quad (\text{C3})$$

where the second line above is the response function, and $f(E_{p,p'})$ being the Maxwell-Boltzmann distributions w.r.t. the core temperature T_c . For non-degenerate medium, there exists little Pauli-blocking from the final states, so $1 - f(E_{p'}) \simeq 1$. In turn, the rate of energy loss is given by

$$\Phi = 2 \int \frac{d^3 k'}{(2\pi)^3} S(q_0, q) \times (E_i - E_f) , \quad (\text{C4})$$

where k' is integrated from 0 to k .

Using this we can write down the time taken to thermalize with the celestial body, i.e. to reach a final energy $E_f = 3/2 T_c$ starting with an initial kinetic energy $E_i = m_\chi v_{\text{esc}}^2/2$:

$$\tau_{\text{therm}} = - \int_{E_i}^{E_f} \frac{dE_i}{\Phi} . \quad (\text{C5})$$

Integrating Eq. (C3) over p' , the response function becomes

$$S(q_0, q) = \int \frac{d^3p}{(2\pi)^{22}} \frac{|\mathcal{M}|^2}{16m_N^2 m_\chi^2} \delta^3 \delta(q_0 - E_p + E_{p'}) f(E_p), \quad (\text{C6})$$

where $E_k = E_{k'} = m_\chi$ and $E_p = E_{p'} = m_N$ have been taken in the denominator, while for the numerator we use $E_p = m_N + p^2/2m_N$ and $E_{p'} = m_N + p'^2/2m_N$. Moreover, the δ^3 enforces momentum conservation, $\mathbf{q} = \mathbf{p}' - \mathbf{p}$, and the energy delta-function is recast in terms of angle between the incoming nuclei and the momentum transfer as shown in Ref. [100], yielding

$$S(q_0, q) \approx \int \frac{dp d\cos\theta}{(2\pi)^{22}} 2\pi p^2 \frac{|\mathcal{M}|^2}{16m_N^2 m_\chi^2} e^{\bar{\mu}/T_c} e^{-p^2/2m_N T_c} \frac{m_N}{|p||q|} \delta(\cos\theta - \cos\theta_0) \Theta(p^2 - p_-^2), \quad (\text{C7})$$

along with

$$\cos\theta_0 = \frac{m_N}{|p||q|} \left(q_0 - \frac{q^2}{2m_N} \right) \quad \text{and} \quad p_-^2 = \frac{m_N^2}{q^2} \left(q_0 - \frac{q^2}{2m_N} \right)^2. \quad (\text{C8})$$

Integrating the above equation we get

$$S(q_0, q) \approx \frac{|\mathcal{M}|^2}{64\pi m_\chi^2} \frac{T_c}{|q|} e^{\bar{\mu}/T_c} e^{-p_-^2/2m_N T_c}. \quad (\text{C9})$$

Taking the Higgs-mixing model introduced in the main text, the squared amplitude for scattering on nucleon in the non-relativistic limit reads

$$|\mathcal{M}|^2 = g_s^2 \cos^2_{\theta_\phi} \sin^2_{\theta_\phi} \frac{m_N^2 f_N^2}{v_H^2} \frac{m_\chi^2 m_N^2}{\left(q_0^2 - q^2 - m_\phi^2 \right)^2}, \quad (\text{C10})$$

which, in the limit of small energy transfer, corresponds to DM-nuclei scattering cross section of

$$\sigma_{\chi N} = g_s^2 \cos^2_{\theta_\phi} \sin^2_{\theta_\phi} \frac{1}{16\pi(m_\chi + m_N)^2} \frac{m_N^2 f_N^2}{v_H^2} \frac{m_\chi^2 m_N^2}{m_\phi^4}. \quad (\text{C11})$$

The k' integral is recast in terms of momentum transfer and energy transfer. The limits of integration are $0 < q_0 < E_k$ and $q_0 < q < 2E_k - q_0$. Therefore the energy loss rate for a particle with initial momenta k is

$$\frac{d\Gamma}{dq_0} \Delta E = \int \frac{dq}{(2\pi)^2} q \frac{E_{k'}}{E_k} S(q_0, q) (E_k - E_{k'}) = \int \frac{dq}{(2\pi)^2} q \frac{E_k - q_0}{E_k} S(q_0, q) q_0. \quad (\text{C12})$$

In the non-degenerate limit the above equation factorizes. Hence the total rate is proportional to cross section on one target particle times their number density [100]. The corresponding numerical results are shown in the right panel of Fig. 7, showing that the thermalization can be reached within the lifetime of the Sun, even with very tiny mixing angles. Including the DM self-interactions would further reduce the time scale of thermalization.

[1] J. D. March-Russell and S. M. West, *Phys. Lett. B* **676**, 133 (2009), [arXiv:0812.0559 \[astro-ph\]](#).

- [2] M. Pospelov and A. Ritz, *Phys. Lett. B* **671**, 391 (2009), [arXiv:0810.1502 \[hep-ph\]](#).
- [3] W. Shepherd, T. M. P. Tait, and G. Zaharijas, *Phys. Rev. D* **79**, 055022 (2009), [arXiv:0901.2125 \[hep-ph\]](#).
- [4] R. Laha and E. Braaten, *Phys. Rev. D* **89**, 103510 (2014), [arXiv:1311.6386 \[hep-ph\]](#).
- [5] B. von Harling and K. Petraki, *JCAP* **12**, 033 (2014), [arXiv:1407.7874 \[hep-ph\]](#).
- [6] K. Petraki, L. Pearce, and A. Kusenko, *JCAP* **07**, 039 (2014), [arXiv:1403.1077 \[hep-ph\]](#).
- [7] K. Petraki, M. Postma, and M. Wiechers, *JHEP* **06**, 128 (2015), [arXiv:1505.00109 \[hep-ph\]](#).
- [8] L. Pearce, K. Petraki, and A. Kusenko, *Phys. Rev. D* **91**, 083532 (2015), [arXiv:1502.01755 \[hep-ph\]](#).
- [9] R. Laha, *Phys. Rev. D* **92**, 083509 (2015), [arXiv:1505.02772 \[hep-ph\]](#).
- [10] H. An, B. Echenard, M. Pospelov, and Y. Zhang, *Phys. Rev. Lett.* **116**, 151801 (2016), [arXiv:1510.05020 \[hep-ph\]](#).
- [11] H. An, M. B. Wise, and Y. Zhang, *Phys. Rev. D* **93**, 115020 (2016), [arXiv:1604.01776 \[hep-ph\]](#).
- [12] H. An, M. B. Wise, and Y. Zhang, *Phys. Lett. B* **773**, 121 (2017), [arXiv:1606.02305 \[hep-ph\]](#).
- [13] X.-J. Bi, Z. Kang, P. Ko, J. Li, and T. Li, *Phys. Rev. D* **95**, 043540 (2017), [arXiv:1602.08816 \[hep-ph\]](#).
- [14] C. Kouvaris, K. Langæble, and N. G. Nielsen, *JCAP* **10**, 012 (2016), [arXiv:1607.00374 \[hep-ph\]](#).
- [15] M. Cirelli, P. Panci, K. Petraki, F. Sala, and M. Taoso, *JCAP* **05**, 036 (2017), [arXiv:1612.07295 \[hep-ph\]](#).
- [16] P. Asadi, M. Baumgart, P. J. Fitzpatrick, E. Krupczak, and T. R. Slatyer, *JCAP* **02**, 005 (2017), [arXiv:1610.07617 \[hep-ph\]](#).
- [17] K. Petraki, M. Postma, and J. de Vries, *JHEP* **04**, 077 (2017), [arXiv:1611.01394 \[hep-ph\]](#).
- [18] E. Johnson, E. Braaten, and H. Zhang, *PoS ICHEP2016*, 210 (2016), [arXiv:1611.06212 \[hep-ph\]](#).
- [19] A. Mitridate, M. Redi, J. Smirnov, and A. Strumia, *JCAP* **05**, 006 (2017), [arXiv:1702.01141 \[hep-ph\]](#).
- [20] I. Baldes, M. Cirelli, P. Panci, K. Petraki, F. Sala, and M. Taoso, *SciPost Phys.* **4**, 041 (2018), [arXiv:1712.07489 \[hep-ph\]](#).
- [21] L. Pearce and A. Kusenko, *Phys. Rev. D* **87**, 123531 (2013), [arXiv:1303.7294 \[hep-ph\]](#).
- [22] R. Mahbubani, M. Redi, and A. Tesi, *Phys. Rev. D* **101**, 103037 (2020), [arXiv:1908.00538 \[hep-ph\]](#).
- [23] R. Mahbubani, M. Redi, and A. Tesi, *JCAP* **02**, 039 (2021), [arXiv:2007.07231 \[hep-ph\]](#).
- [24] J. Chen, Z.-L. Liang, Y.-L. Wu, and Y.-F. Zhou, *JCAP* **12**, 021 (2015), [arXiv:1505.04031 \[hep-ph\]](#).
- [25] J. L. Feng, J. Smolinsky, and P. Tanedo, *Phys. Rev. D* **93**, 115036 (2016), [Erratum: *Phys.Rev.D* **96**, 099903 (2017)], [arXiv:1602.01465 \[hep-ph\]](#).
- [26] C. Arina, M. Backović, J. Heisig, and M. Lucente, *Phys. Rev. D* **96**, 063010 (2017), [arXiv:1703.08087 \[astro-ph.HE\]](#).
- [27] R. K. Leane, K. C. Y. Ng, and J. F. Beacom, *Phys. Rev. D* **95**, 123016 (2017), [arXiv:1703.04629 \[astro-ph.HE\]](#).
- [28] M. Lucente, C. Arina, M. Backović, and J. Heisig, *PoS EPS-HEP2017*, 628 (2017), [arXiv:1710.03947 \[hep-ph\]](#).
- [29] C. Niblaeus, A. Beniwal, and J. Edsjo, *JCAP* **11**, 011 (2019), [arXiv:1903.11363 \[astro-ph.HE\]](#).

- [30] A. Cuoco, P. De La Torre Luque, F. Gargano, M. Gustafsson, F. Loparco, M. N. Mazziotta, and D. Serini, *Phys. Rev. D* **101**, 022002 (2020), [arXiv:1912.09373 \[astro-ph.HE\]](#).
- [31] M. N. Mazziotta, F. Loparco, D. Serini, A. Cuoco, P. De La Torre Luque, F. Gargano, and M. Gustafsson, *Phys. Rev. D* **102**, 022003 (2020), [arXiv:2006.04114 \[astro-ph.HE\]](#).
- [32] B. Dasgupta, A. Gupta, and A. Ray, *JCAP* **10**, 023 (2020), [arXiv:2006.10773 \[hep-ph\]](#).
- [33] N. F. Bell, J. B. Dent, and I. W. Sanderson, *Phys. Rev. D* **104**, 023024 (2021), [arXiv:2103.16794 \[hep-ph\]](#).
- [34] R. Garani and S. Palomares-Ruiz, *JCAP* **05**, 042 (2022), [arXiv:2104.12757 \[hep-ph\]](#).
- [35] A. A. Abud *et al.* (DUNE), *JCAP* **10**, 065 (2021), [arXiv:2107.09109 \[hep-ex\]](#).
- [36] R. K. Leane, T. Linden, P. Mukhopadhyay, and N. Toro, *Phys. Rev. D* **103**, 075030 (2021), [arXiv:2101.12213 \[astro-ph.HE\]](#).
- [37] R. Abbasi *et al.* (IceCube), *Phys. Rev. D* **105**, 062004 (2022), [arXiv:2111.09970 \[astro-ph.HE\]](#).
- [38] N. F. Bell, M. J. Dolan, and S. Robles, *JCAP* **11**, 004 (2021), [arXiv:2107.04216 \[hep-ph\]](#).
- [39] M. Zakeri and Y.-F. Zhou, *JCAP* **04**, 026 (2022), [arXiv:2109.11662 \[hep-ph\]](#).
- [40] D. Bose, T. N. Maity, and T. S. Ray, *Phys. Rev. D* **105**, 123013 (2022), [arXiv:2112.08286 \[hep-ph\]](#).
- [41] T. N. Maity, A. K. Saha, S. Mondal, and R. Laha, (2023), [arXiv:2308.12336 \[hep-ph\]](#).
- [42] M. I. Gresham and K. M. Zurek, *Phys. Rev. D* **99**, 083008 (2019), [arXiv:1809.08254 \[astro-ph.CO\]](#).
- [43] R. Garani, M. H. G. Tytgat, and J. Vandecasteele, *Phys. Rev. D* **106**, 116003 (2022), [arXiv:2207.06928 \[hep-ph\]](#).
- [44] W. H. Press and D. N. Spergel, *Astrophys. J.* **296**, 679 (1985).
- [45] K. Griest and D. Seckel, *Nucl. Phys. B* **283**, 681 (1987), [Erratum: *Nucl.Phys.B* 296, 1034–1036 (1988)].
- [46] M. B. Wise and Y. Zhang, *JHEP* **02**, 023 (2015), [Erratum: *JHEP* 10, 165 (2015)], [arXiv:1411.1772 \[hep-ph\]](#).
- [47] E. Hardy, R. Lasenby, J. March-Russell, and S. M. West, *JHEP* **06**, 011 (2015), [arXiv:1411.3739 \[hep-ph\]](#).
- [48] M. I. Gresham, H. K. Lou, and K. M. Zurek, *Phys. Rev. D* **97**, 036003 (2018), [arXiv:1707.02316 \[hep-ph\]](#).
- [49] M. I. Gresham, H. K. Lou, and K. M. Zurek, *Phys. Rev. D* **96**, 096012 (2017), [arXiv:1707.02313 \[hep-ph\]](#).
- [50] D. N. Spergel and W. H. Press, *Astrophys. J.* **294**, 663 (1985).
- [51] M. Asplund, N. Grevesse, A. Sauval, and P. Scott, *Ann. Rev. Astron. Astrophys.* **47**, 481 (2009), [arXiv:0909.0948 \[astro-ph.SR\]](#).
- [52] R. Garani and S. Palomares-Ruiz, *JCAP* **05**, 007 (2017), [arXiv:1702.02768 \[hep-ph\]](#).
- [53] A. Bottino, G. Fiorentini, N. Fornengo, B. Ricci, S. Scopel, and F. L. Villante, *Phys. Rev. D* **66**, 053005 (2002), [arXiv:hep-ph/0206211](#).
- [54] J. D. Lewin and P. F. Smith, *Astropart. Phys.* **6**, 87 (1996).

- [55] G. Duda, A. Kemper, and P. Gondolo, *JCAP* **04**, 012 (2007), [arXiv:hep-ph/0608035](#).
- [56] M. B. Wise and Y. Zhang, *Phys. Rev. D* **90**, 055030 (2014), [Erratum: *Phys.Rev.D* 91, 039907 (2015)], [arXiv:1407.4121 \[hep-ph\]](#).
- [57] S. Tulin, H.-B. Yu, and K. M. Zurek, *Phys. Rev. D* **87**, 115007 (2013), [arXiv:1302.3898 \[hep-ph\]](#).
- [58] B. Colquhoun, S. Heeba, F. Kahlhoefer, L. Sagunski, and S. Tulin, *Phys. Rev. D* **103**, 035006 (2021), [arXiv:2011.04679 \[hep-ph\]](#).
- [59] L. D. Landau and E. M. Lifshits, *Quantum Mechanics*, Course of Theoretical Physics, Vol. v.3 (Butterworth-Heinemann, Oxford, 1991).
- [60] S. A. Khrapak, A. V. Ivlev, G. E. Morfill, and S. K. Zhdanov, *Phys. Rev. Lett.* **90**, 225002 (2003).
- [61] S. Khrapak, A. Ivlev, G. Morfill, S. Zhdanov, and H. Thomas, *IEEE Transactions on Plasma Science* **32**, 555 (2004).
- [62] A. R. Zentner, *Phys. Rev. D* **80**, 063501 (2009), [arXiv:0907.3448 \[astro-ph.HE\]](#).
- [63] A. Ibarra, S. Lopez Gehler, and M. Pato, *JCAP* **07**, 043 (2012), [arXiv:1205.0007 \[hep-ph\]](#).
- [64] E. Richard *et al.* (Super-Kamiokande), *Phys. Rev. D* **94**, 052001 (2016), [arXiv:1510.08127 \[hep-ex\]](#).
- [65] K. Abe *et al.* (Super-Kamiokande), *Phys. Rev. D* **104**, 122002 (2021), [arXiv:2109.11174 \[astro-ph.HE\]](#).
- [66] S. Abe *et al.* (KamLAND), *Astrophys. J.* **925**, 14 (2022), [arXiv:2108.08527 \[astro-ph.HE\]](#).
- [67] G. Battistoni, A. Ferrari, T. Montaruli, and P. R. Sala, *Astropart. Phys.* **23**, 526 (2005).
- [68] B. Zhou and J. F. Beacom, (2023), [arXiv:2311.05675 \[hep-ph\]](#).
- [69] A. M. Suliga and J. F. Beacom, *Phys. Rev. D* **108**, 043035 (2023), [arXiv:2306.11090 \[hep-ph\]](#).
- [70] M. Honda, M. Sajjad Athar, T. Kajita, K. Kasahara, and S. Midorikawa, *Phys. Rev. D* **92**, 023004 (2015), [arXiv:1502.03916 \[astro-ph.HE\]](#).
- [71] G. Krnjaic, *Phys. Rev. D* **94**, 073009 (2016), [arXiv:1512.04119 \[hep-ph\]](#).
- [72] M. W. Winkler, *Phys. Rev. D* **99**, 015018 (2019), [arXiv:1809.01876 \[hep-ph\]](#).
- [73] S. Matsumoto, Y.-L. S. Tsai, and P.-Y. Tseng, *JHEP* **07**, 050 (2019), [arXiv:1811.03292 \[hep-ph\]](#).
- [74] D. Harvey, R. Massey, T. Kitching, A. Taylor, and E. Tittley, *Science* **347**, 1462 (2015), [arXiv:1503.07675 \[astro-ph.CO\]](#).
- [75] K. Bondarenko, A. Boyarsky, T. Bringmann, and A. Sokolenko, *JCAP* **04**, 049 (2018), [arXiv:1712.06602 \[astro-ph.CO\]](#).
- [76] D. Harvey, A. Robertson, R. Massey, and I. G. McCarthy, *Mon. Not. Roy. Astron. Soc.* **488**, 1572 (2019), [arXiv:1812.06981 \[astro-ph.CO\]](#).
- [77] L. Sagunski, S. Gad-Nasr, B. Colquhoun, A. Robertson, and S. Tulin, *JCAP* **01**, 024 (2021), [arXiv:2006.12515 \[astro-ph.CO\]](#).
- [78] D. Cross *et al.* (DES), (2023), [arXiv:2304.10128 \[astro-ph.CO\]](#).
- [79] S. Tulin and H.-B. Yu, *Phys. Rept.* **730**, 1 (2018), [arXiv:1705.02358 \[hep-ph\]](#).
- [80] S. Adhikari *et al.*, (2022), [arXiv:2207.10638 \[astro-ph.CO\]](#).
- [81] M. Vogelsberger, J. Zavala, and A. Loeb, *Mon. Not. Roy. Astron. Soc.* **423**, 3740 (2012), [arXiv:1201.5892 \[astro-ph.CO\]](#).

- [82] J. Zavala, M. Vogelsberger, and M. G. Walker, *Mon. Not. Roy. Astron. Soc.* **431**, L20 (2013), [arXiv:1211.6426 \[astro-ph.CO\]](#).
- [83] O. D. Elbert, J. S. Bullock, S. Garrison-Kimmel, M. Rocha, J. Oñorbe, and A. H. G. Peter, *Mon. Not. Roy. Astron. Soc.* **453**, 29 (2015), [arXiv:1412.1477 \[astro-ph.GA\]](#).
- [84] T. Ren, A. Kwa, M. Kaplinghat, and H.-B. Yu, *Phys. Rev. X* **9**, 031020 (2019), [arXiv:1808.05695 \[astro-ph.GA\]](#).
- [85] E. Aprile *et al.* (XENON), *Phys. Rev. Lett.* **121**, 111302 (2018), [arXiv:1805.12562 \[astro-ph.CO\]](#).
- [86] P. Athron *et al.* (GAMBIT), *Eur. Phys. J. C* **79**, 38 (2019), [arXiv:1808.10465 \[hep-ph\]](#).
- [87] J. Aalbers *et al.* (LZ), *Phys. Rev. Lett.* **131**, 041002 (2023), [arXiv:2207.03764 \[hep-ex\]](#).
- [88] K. Agashe, Y. Cui, L. Necib, and J. Thaler, *JCAP* **10**, 062 (2014), [arXiv:1405.7370 \[hep-ph\]](#).
- [89] M. Cirelli, G. Corcella, A. Hektor, G. Hutsi, M. Kadastik, P. Panci, M. Raidal, F. Sala, and A. Strumia, *JCAP* **03**, 051 (2011), [Erratum: *JCAP* 10, E01 (2012)], [arXiv:1012.4515 \[hep-ph\]](#).
- [90] C. A. Argüelles, A. Diaz, A. Kheirandish, A. Olivares-Del-Campo, I. Safa, and A. C. Vincent, *Rev. Mod. Phys.* **93**, 035007 (2021), [arXiv:1912.09486 \[hep-ph\]](#).
- [91] G. Elor, N. L. Rodd, T. R. Slatyer, and W. Xue, *JCAP* **06**, 024 (2016), [arXiv:1511.08787 \[hep-ph\]](#).
- [92] X. Chu, C. Garcia-Cely, and H. Murayama, *JCAP* **06**, 043 (2020), [arXiv:1908.06067 \[hep-ph\]](#).
- [93] D. Yang and H.-B. Yu, *JCAP* **09**, 077 (2022), [arXiv:2205.03392 \[astro-ph.CO\]](#).
- [94] S. Cassel, *J. Phys. G* **37**, 105009 (2010), [arXiv:0903.5307 \[hep-ph\]](#).
- [95] L. Landau and E. Lifshitz, *Mechanics: Volume 1*, Course of theoretical physics (Elsevier Science, 1976).
- [96] C. Kouvaris and P. Tinyakov, *Phys. Rev. D* **83**, 083512 (2011), [arXiv:1012.2039 \[astro-ph.HE\]](#).
- [97] P. Tinyakov, M. Pshirkov, and S. Popov, *Universe* **7**, 401 (2021), [arXiv:2110.12298 \[astro-ph.HE\]](#).
- [98] B. Bertoni, A. E. Nelson, and S. Reddy, *Phys. Rev. D* **88**, 123505 (2013), [arXiv:1309.1721 \[hep-ph\]](#).
- [99] R. Garani, A. Gupta, and N. Raj, *Phys. Rev. D* **103**, 043019 (2021), [arXiv:2009.10728 \[hep-ph\]](#).
- [100] S. Reddy, M. Prakash, and J. M. Lattimer, *Phys. Rev. D* **58**, 013009 (1998), [arXiv:astro-ph/9710115](#).